UNIVERSITY OF CALIFORNIA

Los Angeles

Dissecting the roles of IRFs in *de novo* enhancer formation in macrophages

A dissertation submitted in partial satisfaction of the requirements for the degree

Doctor of Philosophy in Molecular and Medical Pharmacology

by

Carolina Chavez

2023

ABSTRACT OF THE DISSERTATION

Dissecting the roles of IRFs in

de novo enhancer formation in macrophages

by

Carolina Chavez

Doctor of Philosophy in Molecular and Medical Pharmacology

University of California, Los Angeles, 2023

Professor Alexander Hoffmann, Co-Chair

Professor Thomas G. Graeber, Co-Chair

Macrophages exposed to immune stimuli reprogram their epigenomes to alter subsequent functions. Here, we have dissected the roles of interferon regulatory factors (IRFs) in innate immune *de novo* enhancer formation. We found that upon transient endotoxin exposure, such enhancers may remain poised for days. Endotoxin-activated IRF3 induces only a small number of *de novo* enhancers directly, but it is indirectly required for the formation of a large number of enhancers *via* type I interferon-induced ISGF3. However, ISGF3 is unable to trigger enhancer formation by itself – it must cooperate with NFκB-induced IRF1. In type II IFN, IRF1 induces enhancer formation by cooperating with GAF. We found that IRF1 is particularly required in locations that show less chromatin accessibility in naïve macrophages, and a fine timecourse revealed that IRF1 is required for the initial opening of chromatin before ISGF3 extends it and recruits enzymes to deposit H3K4me1 marks. Our results reveal an IRF1-mediated combinatorial logic gate to provide innate immune memory formation in cells exposed

to pathogen or activated IFNγ-secreting T cells, but not bystander macrophages that benefit from the transient anti-viral message of type I interferon.

The dissertation of Carolina Chavez is approved.

Quen J. Cheng

Stephen Smale

Maureen A. Su

Alexander Hoffmann, Committee Co-Chair

Thomas G. Graeber, Committee Co-Chair

University of California, Los Angeles

2023

TABLE OF CONTENTS

LIST OF FIGURES

ACKNOWLEDGEMENTS

Carolina Chavez, Quen Cheng and Alexander Hoffmann conceived and designed the study presented in this thesis. Carolina Chavez performed most experiments and analyzed all data. Kelly Lin contributed experimental work. Alexis Malveaux contributed to analysis of RNA-seq data. Stephen Smale contributed to the Lipid A-treated ATAC-seq data of WT and *Irf3*$^{-/-}$ BMDMs. Studies were directed by Quen Cheng and Alexander Hoffmann.

This project was supported by funds to Alexander Hoffmann (R01AI132835) and Quen Cheng (K08AI168567). Carolina Chavez was supported by the UCLA Molecular Pathogenesis Training Grant (PIs Patricia Johnson and Peter Bradley). Alexis Malveaux was supported by the UCLA URSP Hilton Endowment Scholarship. We acknowledge expert services by UCLA's Technology Center for Genomics and Bioinformatics (TCGB) and the Division of Laboratory Animal Medicine (DLAM). We thank all lab members for insightful discussions.

VITA

EDUCATION

University of California Los Angeles, Los Angeles, CA — 2018-2023 (Expected)

Doctor of Philosophy in Molecular and Medical Pharmacology

University of California San Diego, San Diego, CA — 2015-2017

Bachelor of Science in Biochemistry and Cell Biology

AWARDS

Microbial Pathogenesis Training Grant — 2022-2023

Cota-Robles Fellowship — 2018-2019; 2021-2022

NIH/NIGMS Diversity Supplement Grant Award — 2017-2018

McNair Scholar — 2016-2017

PUBLICATIONS

Chavez C, Lin K, Malveaux A, Cheng Q and Hoffmann A. IRF1 Acts in Concert with ISGF3 and GAF to Create de novo Enhancers in Murine Macrophages. *In preparation*

Chavez C, Cruz-Becerra G, Fei J, Kassavetis GA, Kadonaga JT. The tardigrade damage suppressor protein binds to nucleosomes and protects DNA from hydroxyl radicals. Elife. 2019;8:e47682. Published 2019 Oct 1. doi:10.7554/eLife.47682

TRAINEES

Alexis Malveaux, Undergraduate Researcher — 2021-2023

Kelly Lin, Undergraduate Researcher — 2021-2023

CHAPTER 1: INTRODUCTION

CHAPTER 1: INTRODUCTION

1.1 Innate immune memory

Immune responses are classically divided into innate and adaptive immunity. Innate immune cells react rapidly to pathogen associated molecular patterns (PAMPs) or damage associated molecular patterns (DAMPs) and can in turn coordinate the activation and recruitment of adaptive immune cells (Sheu et al. 2019). Responses by adaptive immune cells are slower to develop but result in immunological memory, resulting in a stronger and more rapid response to subsequent exposure to the same pathogen (Charles A Janeway et al. 2001). Macrophages are a critical cell type of the innate immune system that can respond to PAMPs and DAMPs by inducing stimulus-specific signaling programs which will result in the activation of transcription factors, secretion of cytokines, and transcription of genes that will facilitate pathogen clearance or activation of the adaptive immune system (Ahmed et al. 2022).

While adaptive immune cells can develop pathogen-specific and long-term immune responses, the dogma that only adaptive immune cells can build memory has been challenged by studies showing that innate immune cells can mount resistance to reinfection (Netea et al. 2016). This innate immune memory in macrophages can be observed in the well-established phenomenon of endotoxin-induced tolerance, a transient unresponsive state where cells are unable to respond to further challenges (Biswas and Lopez-Collazo 2009), or the potentiation of gene expression to subsequent immune challenges (Rodriguez et al. 2019) (Figure 1.1). Evidence of this reprogramming has been observed in macrophages by signaling through pathogen recognition receptors (PRRs) such as toll-like receptors (TLRs) or interferon (IFN) receptors for Type I (IFNβ) or Type II (IFNγ) IFNs (Cheng et al. 2019; Kang et al. 2019; Foster et al. 2007; van der Heijden et al. 2018).

Early evidence of trained immunity was observed in mice that demonstrated protection after a β-glucan injection, subsequently surviving a lethal injection of *Staphylococcus aureus* (Bistoni et al. 1986). Since then, multiple studies in humans have revealed heterologous protection by β-glucan vaccine to influenza and other viral infections, or by vaccines against measles-mumps-Rubella (MMR), oral polio vaccine (OPV), or influenza (Kaufmann et al. 2022; Ziogas and Netea 2022). The innate immune memory associated with these responses has been correlated with the epigenetic reprogramming of monocytes and macrophages (Foster et al. 2007; Ostuni et al. 2013; Yoshida et al. 2015; Quintin et al. 2012; Saeed et al. 2014). Clinically, epigenetic targeting of these processes has been explored to ameliorate inflammation and tissue damage in rheumatoid arthritis, asthma, encephalomyelitis, chronic kidney disease, and cancer (Rodriguez et al. 2019). This dissertation will focus on the stimulus-responsive transcription factors that elicit epigenetic reprogramming of macrophages by IFN or TLR signaling that lead to innate immune memory.

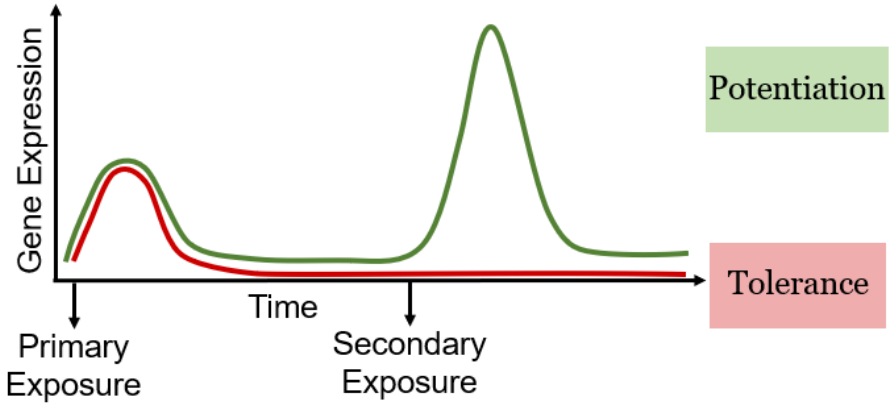

Figure 1.1. Schematic diagram of innate immune memory. Epigenetic reprogramming *via* the stimulus-responsive generation of *de novo* enhancers leads to potentiated gene expression responses to subsequent heterologous stimulation. In contrast, epigenetic reprogramming via the stimulus-responsive deposition of repressive marks may lead to dampening of the inflammatory response, also known as tolerance.

1.2 Type I and type II interferon signaling

The interferons (IFNs) constitute a family of cytokines that were discovered because of their potent antiviral properties (Honda et al. 2006). Subsequent classification has delineated them into Type I (IFNα/β), Type II (IFNγ) and Type III (λ) IFNs, each contributing uniquely to cellular processes such as cell proliferation, apoptosis, inflammation, and adaptive immunity (Michalska et al. 2018). Although Type I and Type II IFNs utilize distinct receptors, both activate Janus kinase (JAK)-dependent phosphorylation of signal transducer and activator of transcription (STAT) and induce expression of interferon stimulated genes (ISGs).

Type I, including IFNα and IFNβ, are elicited in response to microbial stimuli detected by pattern recognition receptors (PRRs). IFNβ is secreted by infected cells to induce a gene expression program that confers an antimicrobial state in both the infected and neighboring cells (Ivashkiv and Donlin 2014). The binding of IFNβ to its receptor IFNAR1 and IFNAR2 activates JAK1 and TYK2 kinases, leading to the phosphorylation of STAT1 and STAT2 (Figure 1.2). This results in the formation of a heterotrimeric complex with IRF9, known as ISGF3, which binds to the IFN-stimulated response element (ISRE) sequence, GAAANNGAAACT (Cohen et al. 1988; Schmid et al. 2010). In macrophages, innate defenses in the infected cells and neighboring cells is dominated by IFNβ responsive ISGF3 (Ourthiague et al. 2015).

Type II IFN, predominantly IFNγ, is produced in response to foreign antigens by T lymphocytes and natural killer (NK) cells (Michalska et al. 2018). Macrophages conditioned with IFNγ have been termed “classically activated” M1 macrophages and are skewed towards a pro-inflammatory phenotype (Murray and Wynn 2011). Binding of IFNγ to receptor complex IFNGR1 and IFNGR2 activates JAK1 and JAK2 kinases, leading to the phosphorylation of STAT1 and formation of homodimer of STAT1 (GAF) (Figure 1.2). GAF binds to the γ-IFN activated site GAS, the palindromic sequence TTTC$(N)_{2-4}$GAAA (Decker et al. 1997; Ramsauer et al. 2007; Sekrecka et al. 2023). Notably, however, high doses of type I IFN can also activate GAF

(Kishimoto et al. 2021) (Figure 1.2). Whether high doses of IFNγ can also activate ISGF3 in macrophages has not been reported.

IFNγ-induced STAT1 activation and the downstream transcriptional network lead to remodeling of the epigenome that alters gene transcription (Ivashkiv 2018). IFNγ induces formation of several hundred of enhancers that persist for at least 48 hours after removal of IFNγ (Ostuni et al. 2013). This priming of regulatory elements allows for sustained transcriptional responses to a secondary stimulus, thereby conferring short-term transcriptional memory. The exploration of mechanisms underlying enhancer formation by interferons holds significant interest, offering potential avenues for identifying therapeutic targets.

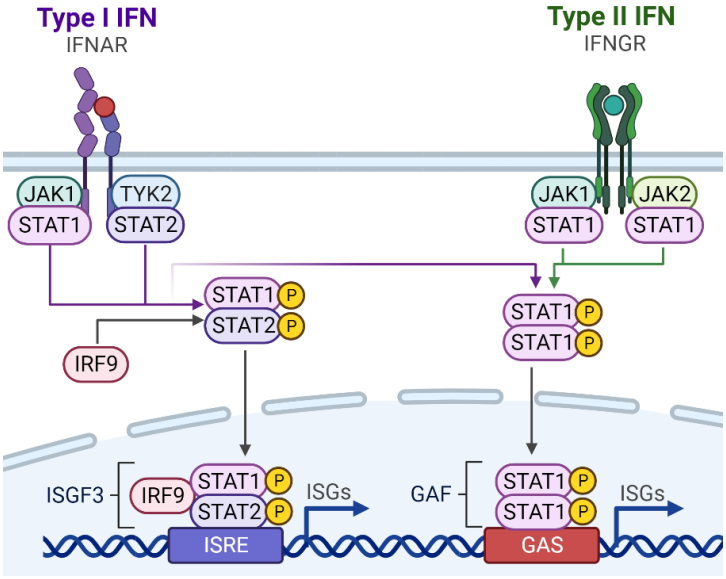

Figure 1.2. Type I and Type II IFN signaling pathways. Type I IFNs, such as IFNβ, signals through IFNAR to activate ISGF3, and at high enough doses, it can also activate GAF. Type II IFNs, such as IFNγ, signals through IFNGR to activate GAF. ISGF3 or GAF translocate to the nucleus to bind to ISRE or GAS sequences, respectively, and activate transcription of ISGs. Figure created with Biorender.

1.3 TLR4 signaling

Toll-like receptors (TLRs) are type I transmembrane proteins that recognize a variety of PAMPs and elicit immune responses, including the secretion of IFNβ. To date, there are 10 known TLRs in humans and 12 in mice (Tamura et al. 2008). All TLRs initiate downstream signaling by recruiting adaptor proteins, such as myeloid differentiation primary-response protein 88 (MyD88) and TIR domain-containing adaptor inducing IFNβ (TRIF) (Tamura et al. 2008).

TLR4 is a cell surface receptor that recognizes endotoxins from gram-negative bacteria, such as the lipopolysaccharide LPS. Notably, TLR4 is unique among TLRs in its ability to activate both, the MyD88 and the TRIF pathways, which in turn activate downstream families of transcription factors NFκB and IRFs, respectively (Tamura et al. 2008). TRIF recruits non-canonical IKKs known as TBK1 and IKKε via TRAF3 to activate the IRF3 transcription factor. Once phosphorylated and dimerized, IRF3 translocates to the nucleus to induce the transcription of IFNβ and other genes (Kawai and Akira 2010).

The detection of endotoxin triggers a robust inflammatory response, but excessive inflammation can lead to a state of tolerance (Biswas and Lopez-Collazo 2009). However, the Medzhitov group elucidated two set of gene programs initiated by LPS: the silencing of pro-inflammatory genes and the priming of antimicrobial effectors (Foster et al. 2007). Notably, the promoters of antimicrobial genes exhibit increased tri-methylation of lysine 4 of histone H3 (H3K4me3) and chromatin accessibility, leading to faster and more robust induction of these genes.

Similarly, our studies have also shown that LPS induces mono-methylation of lysine 4 of histone H3 (H3K4me1) at hundreds of genomic locations, an epigenetic mark indicative of enhancers (Cheng et al. 2021). LPS activates NFκB with non-oscillatory dynamics, inducing

hundreds of *de novo* enhancers (Cheng et al. 2021). A second set of hundreds of *de novo* enhancers are associated with ISREs, the cognate motif for IRFs. Which IRF family members regulate *de novo* enhancer formation and subsequent gene expression responses remains unknown.

1.4 Chromatin remodeling of de novo *enhancers*

DNA is organized into nucleosomes wrapped around histone octamers, compacted in the nucleus in the form of chromatin (Chen et al. 2020). Heterochromatin is characterized by tightly compacted nucleosomes that inhibit the entry of transcription factor machinery and gene transcription. Chromatin undergoes structural alterations to “loosen” the DNA from nucleosomes and transition from an inactive to an active transcription state. This is initiated by pioneer factors, transcription factors that can bind to closed chromatin and recruit enzymes that displace nucleosomes or deposit epigenetic marks on nearby core histones or polymerases that initiate gene transcription.

Nucleosome-free regions in functional sequences regulate gene expression; promoters are located proximal to the transcription start site (TSS), while enhancers are distal to genes (Chen et al. 2020). Chromatin in different functional classes are segregated spatially by chromatin associations to nuclear bodies, where active chromatin is typically closer to nuclear speckles (Yildirim et al. 2022). Proximity to nuclear speckles promotes interactions between promoters and enhancers and act as hubs for transcription factor machinery (Kim et al. 2019; Yildirim et al. 2022). One enhancer typically regulates many genes, and one gene is typically regulated by many enhancers. This inherent many-to-many complexity poses challenges in identifying the gene target of a specific enhancer within the regulatory landscape.

Lineage determining transcription factors (LDTFs), such as PU.1, play critical roles in macrophage lineage development and the maintenance of macrophage-specific enhancers (Chen et al. 2020; Mayran and Drouin 2018). Until recently, it was believed that the enhancer repertoire of a differentiated cell is fixed by the presence of LDTFs. However, recent evidence suggests that macrophages can undergo epigenetic reprogramming in response to immune challenges, regulated by signal-dependent transcription factors (SDTFs) (Ostuni et al. 2013; Cheng et al. 2021; Comoglio et al. 2019).

In macrophages, latent or *de novo* enhancers represent chromatinized genomic regions that are opened in response to stimuli, increasing their accessibility and gaining H3K4me1, a marker of enhancers (Ostuni et al. 2013). The formation of *de novo* enhancers in response to cytokines or PAMPs is mediated by stimulus-dependent transcription factors (SDTFs) (Ostuni et al. 2013; Kaikkonen et al. 2013; Comoglio et al. 2019; Cheng et al. 2021). Active enhancers also have H3K27ac marks, while poised enhancers lack this epigenetic mark (Chen et al. 2020). The persistence of H3K4me1 even after removal of the initial activation suggests that this epigenetic memory reprograms the macrophage's subsequent stimulus-responses, potentiating expression of immune response genes (Netea et al. 2016).

The underlying mechanism of *de novo* enhancer formation involves several distinguishable phases (Figure 1.3). First, SDTFs bind to cognate sequences within nucleosomal DNA which might be closed or pre-primed with LDTFs binding (Ostuni et al. 2013). Next, a phase of binding stabilization in conjunction with nucleosomal opening increases chromatin accessibility within minutes, potentially in cooperation with chromatin remodeling and enzymes such as SWI/SNF (SWItch/Sucrose Non-Fermentable) or FACT (Facilitates Chromatin Transcription) (Kim et al. 2022), and pioneer factors such as PU.1. Following this, RNA polymerase II is recruited to transcribe these enhancer regions, referred to as eRNAs (Kaikkonen et al. 2013). Finally, SDTFs may contribute to the recruitment of chromatin modifiers resulting in the deposition of H3K4me1 within hours after stimulation (Figure 1.3) (Mayran and Drouin 2018; Ostuni et al. 2013; Kaikkonen et al. 2013).

Our studies showed that the formation of *de novo* enhancers is stimulus-specific (Cheng et al. 2021). NFκB induces hundreds of *de novo* enhancers, but only when it is activated with non-oscillatory dynamics (Cheng et al. 2021). This dynamic requirement ensures that enhancer formation is restricted to MyD88-mediated signals emanating from bacterial PAMPs, such as LPS, but not, paracrine TNF, which activates NFκB with oscillatory dynamics. A second set of

hundreds of *de novo* enhancers are associated with ISREs, the cognate motif for the family of interferon regulatory factors (IRFs). This dissertation will focus on identifying which IRFs are required for *de novo* enhancer formation.

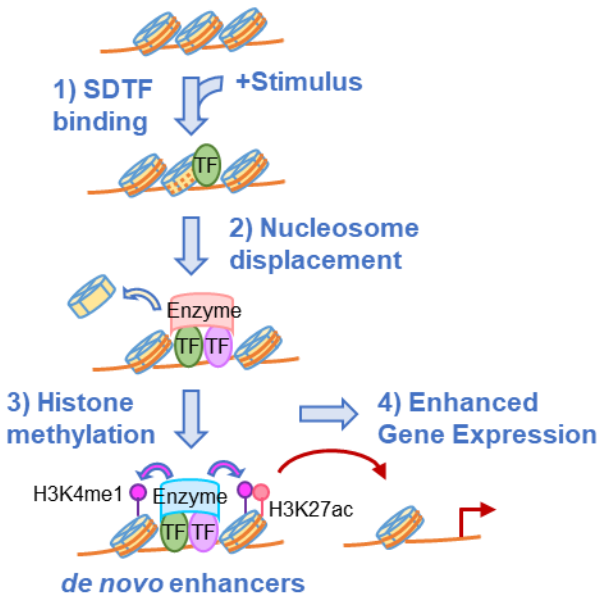

Figure 1.3. Model for *de novo* enhancer formation. Upon stimulation, signal dependent transcription factors (SDTFs) bind to closed and unmarked chromatin. Subsequently, these SDTFs may recruit additional transcription factors (TF) and chromatin modifiers to displace nucleosomes. The recruitment of other enzymes results in deposition of H3K4me1 or H3K27ac, effectively marking the enhancer as active. Active enhancers can potentiate gene expression of target genes.

1.5 The IRF family of transcription factors

The interferon regulatory factors (IRFs) emerged as pivotal regulators of antiviral responses, initially discovered in 1988 (Miyamoto et al. 1988). They comprise nine family members with cell-type specific roles (Zhao et al. 2015; Yanai et al. 2012). Of these, IRF1, IRF3/IRF7, and IRF9 (part of the ISGF3 complex) are relevant for stimulus responses in murine M-CSF-differentiated bone marrow-derived macrophages (BMDMs) (Zhao et al. 2015).

IRF1 was first identified as a transcriptional regulator of type-I IFNs (Fujita et al. 1988), and further studies have revealed a broad function of IRF1 in regulating inflammation, cell growth, apoptosis, and more recently, its influence on metabolic programs, control of the insulin/IGF signaling pathway following SARS-CoV-2 infection, and regulation of immunity to mycobacteria (Tamura et al. 2008; Shi et al. 2011; Shin et al. 2022; Alfarano et al. 2023; Rosain et al. 2023). IRF1 expression is induced by NFκB and GAF, the binding sites for which are found within the promoter region (Taniguchi et al. 2001). Upon TLR4 signaling, IRF1 expression is activated via NFκB, while Type II IFN activates it via GAF (Figure 1.4).

IRF3 and IRF7 are pivotal regulators of IFNβ expression (Honda et al. 2006). IRF3 resides in the cytosol, and upon infection it undergoes phosphorylation, dimerization, and nuclear translocation where it binds to consensus interferon response elements (IREs) to promote gene expression (Honda et al. 2006; Fujii 1999). IFNβ is secreted via IRF3 from infected cells and binds to IFNAR on the same or neighboring cells, which activates downstream transcription factor ISGF3. IRF7 is highly homologous to IRF3, but it is IFN-inducible in an ISGF3-dependent manner (Sato et al. 1998), establishing a potential positive feedback loop wherein IRF3 induces IFNβ which signals the cells to induce IRF7 expression and further activates IFNβ (Sakaguchi et al. 2003). While the first PAMP-responsive IRF is IRF3, activation of ISGF3 dominates the subsequent gene expression response (Ourthiague et al. 2015).

The activation of IRFs downstream of LPS and IFN signaling has been heavily explored (Figure 1.4). Our previous studies determined that about half of the LPS-inducible *de novo* enhancers are associated with ISRE motifs and are absent in an *Irf3*$^{-/-}$*Ifnar*$^{-/-}$ double knockout that is defective in IRF3 and ISGF3 activity. However, a key impediment to dissecting the functional specificity of IRF is that all bind a highly conserved DNA sequence known as the interferon-sensitive response element (ISRE, direct repeats of GAAA), with only minor deviations (Ourthiague et al. 2015), resulting in potential compensation among family members. Furthermore, STAT proteins also bind to GAAA repeats and the STAT1 homodimer (GAF), responsive to IFNγ, binds an inverted repeat of this sequence (GAS element). Recent evidence corroborates our observation that IRFs can remodel the epigenome of macrophages (Song et al. 2021; Platanitis et al. 2022a; Zhang et al. 2015). Yet, the specific roles of IRF1, IRF3, ISGF3, and GAF in the epigenetic reprogramming of PAMP- and IFN-inducible responses is less well understood.

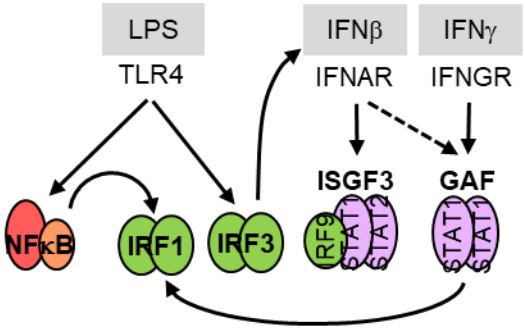

Figure 1.4. Schematic diagram of IRF activation by TLR4 and IFN signaling. TLR4 signaling triggers the activation of IRF3, resulting in the secretion of IFNβ and subsequent activation of ISGF3 *via* IFNAR. IRF1 is activated downstream of TLR4 signaling through NFκB, while it is activated downstream of IFNγ through GAF. High doses of IFNβ induce GAF activation, thereby activating IRF1.

1.6 Summary

Here we combine a genetic approach with biochemical characterization of the IRF signaling network and epigenomic profiling to delineate the roles of IRF family members in *de novo* enhancer formation during the innate immune response. We found that only at a minority of *de novo* enhancers IRF3 acts directly, but its major role is indirect *via* IFNβ induction and consequent ISGF3 activation. However, ISGF3 requires the coordinated function of IRF1, which is activated by NFκB in cells responding to pathogen exposure, but not at IFNβ levels in which only ISGF3 is activated. We thus report a combinatorial requirement for ISRE-driven enhancers that ensures stimulus-specificity in epigenomic reprogramming. Indeed, IRF1 cooperates with GAF to trigger formation of *de novo* enhancers. We conclude that while IRF1 is a versatile chromatin remodeling SDTF, it must function combinatorially with other SDTFs to ensure that long-lasting epigenome remodeling is restricted to cells directly exposed to pathogen or when in proximity to adaptive immune cells secreting IFNy.

CHAPTER 2: RESULTS

CHAPTER 2: RESULTS

2.1. Molecular characteristics of de novo *enhancers induced by endotoxin*

Our previous studies revealed that the endotoxin-induced *de novo* enhancers associated with ISRE motifs were abolished by the combined deficiency of IRF3 and ISGF3 (Cheng et al. 2021). To dissect the contributions of IRF3 and ISGF3 in *de novo* enhancer formation, we stimulated BMDMs generated from WT, *Irf3*$^{-/-}$*Ifnar*$^{-/-}$, *Ifnar*$^{-/-}$, and *Irf3*$^{-/-}$ mice with 100 ng/mL LPS for 8 hours. We performed chromatin immunoprecipitation sequencing (ChIP-seq) using an antibody against H3K4me1 and identified 4800 *de novo* enhancer regions by applying a cutoff for the false discovery rate (FDR) of <0.05 and for the $\log_2$ fold change (LFC) of >0.5 of triplicate data upon LPS stimulation in WT cells. The majority of these H3K4me1 regions were in intergenic and intronic regions, while a vast minority were found in TSS or exonic regions (Figure 2.1A). When considering knockout data, these 4800 *de novo* enhancers clustered into two major groups by unsupervised k-means clustering (Figure 2.1B): cluster 1 (C1) was enriched for IRF motifs whereas cluster 2 (C2) was enriched for NFκB motifs.

Consistent with our previous findings (Cheng et al. 2021), we observed a significant loss of C1 IRF-associated *de novo* enhancer formation in *Irf3*$^{-/-}$*Ifnar*$^{-/-}$ cells that are deficient in both ISGF3 and IRF3 activity (Figure 2.1B). Both, *Ifnar*$^{-/-}$ or *Irf3*$^{-/-}$ single knockouts also showed deficiencies in the formation of C1 IRF-associated *de novo* enhancers (Figure 2.1B), suggesting that both IRF3 and ISGF3 are required for IRF-associated enhancer formation.

To further characterize these *de novo* enhancers, we examined published ChIP-seq datasets of H3K27ac, PU.1, and RNA Polymerase II (RNAPol II) on LPS-stimulated BMDMs (Ostuni et al. 2013). We found that about 80% of IRF-associated *de novo* enhancers acquire the H3K27ac modification at the 4-hour timepoint, with the basal signal detectable in 30% of latent locations (Figure 2.1C). The H3K27ac signal is transient, as it decreases from mean $\log_2$ RPKM

values of 2.7 at 4 hours to 1.6 at the 24-hour timepoint (Figure 2.1C). Similar numbers are observed for the NFκB-regulated enhancers of cluster C2, whereas 88% of promoter regions of LPS-inducible genes (LFC>0.5, data not shown) had detectable H3K27ac modification prior to stimulation (Figure 2.1C). In addition, RNAPol II occupancy at the basal state was higher in promoters (73%) than enhancers (4%) and was recruited similarly to the IRF- and NFκB-associated enhancers at four hours (Figure 2.1D).

Another critical factor of macrophage gene expression is PU.1, which is required for macrophage differentiation, and it establishes macrophage enhancers to enable binding of SDTFs upon stimulation (Ghisletti et al. 2010; Heinz et al. 2010; Ostuni et al. 2013). Examining the endotoxin-induced *de novo* enhancers, we found that PU.1 binding is induced substantially to both C1 and C2 enhancers within 4 hours of LPS stimulation and persists for at least 24 hours (Figure 2.1E). In contrast, PU.1 signals at LPS-inducible promoters are high before stimulation and barely inducible. Collectively, these results suggest that in contrast to LPS-inducible promoters that are “pre-primed” with RNAPol II, PU.1, and H3K27ac, latent *de novo* enhancer regions are in a more inactive state, from which they must be activated by stimulus-induced SDTFs that initiate chromatin remodeling.

To investigate the longevity of the IRF- and NFkB- associated enhancers, we removed the LPS after an 8-hour stimulation and performed H3K4me1 ChIP-seq at different time intervals. Contrary to the transient H3K27ac epigenetic changes, the H3K4me1 marks remained relatively unchanged for at least 6 days post-stimulation in both C1 and C2 *de novo* enhancers (Figure 2.1F). The longer-lasting temporal dynamics of H3K4me1 suggests that these enhancers remain in a “poised” state that allows for activation to subsequent stimulus.

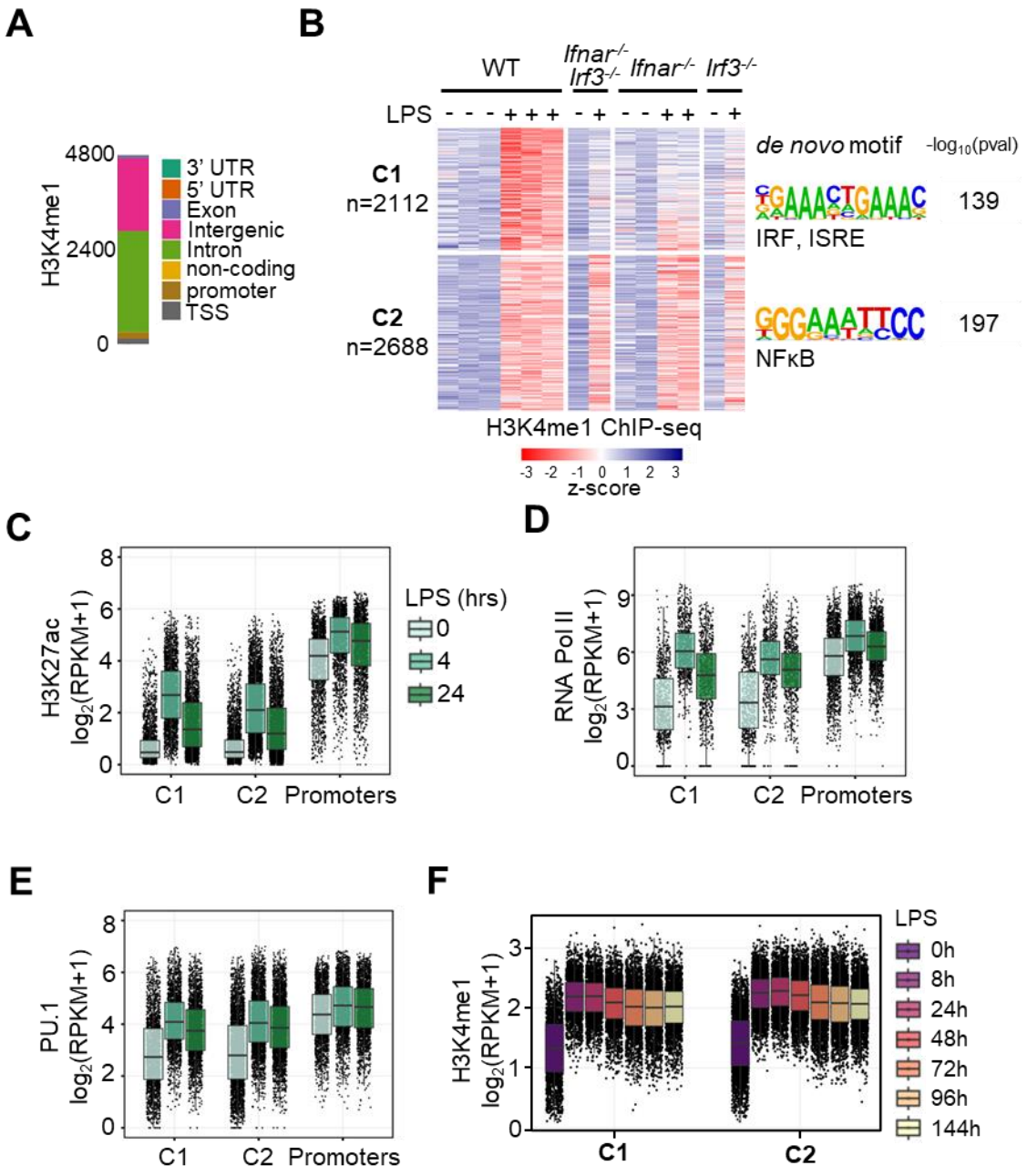

Figure 2.1. Latent *de novo* enhancers are in an inactive state prior to stimulation. (A) Genomic distribution of the H3K4me1 locations (LFC>0.5, FDR<0.05) induced by 8 hours of LPS (100 ng/mL) stimulation in BMDMs. (B) Heatmap of z-scored H3K4me1 ChIP-seq data after 8 hours of LPS stimulation of WT, *Ifnar*$^{-/-}$*Irf3*$^{-/-}$, *Ifnar*$^{-/-}$, or *Irf3*$^{-/-}$ BMDMs. Clusters generated by unsupervised k-means were subjected to *de novo* motif analysis; top enriched sequences

are shown. (C-E) Box plots of $\log_2$ RPKM counts of ChIP-seq data for (C) H3K27ac, (D) RNA Pol II, or (E) PU.1 in the LPS-induced C1 or C2 *de novo* enhancers (GSE38377) or promoter regions of LPS-inducible genes (LFC>0.5). (F) Box plots of $\log_2$ RPKM normalized H3K4me1 ChIP-seq on different time intervals after removal of the 8-hour LPS stimulation.

2.2. Enhancer formation deficiency in Irf3$^{-/-}$ *BMDMs is due to the lack of ISGF3 activity*

Our results suggest that in response to endotoxin exposure, both IRF3 and ISGF3 are required for the formation of IRF-associated *de novo* enhancers. To further address the relative contributions of IRF3 and ISGF3, we investigated their respective roles in opening chromatin at the endotoxin-induced enhancer locations. We stimulated BMDMs for 2 hours with 100 ng/mL of LPS (WT and *Ifnar*$^{-/-}$) or Lipid A (WT and *Irf3*$^{-/-}$) and performed ATAC-seq. Knockouts of either factor showed deficiency in chromatin accessibility upon LPS stimulation of C1 but not C2 enhancers (Figure 2.2A). However, when we analyzed ChIP-seq datasets for IRF3 on LipidA-treated BMDMs (Tong et al. 2016) or for IRF9 in IFNβ-treated BMDMs (Platanitis et al. 2019), we found that while IRF9 was frequently found on C1 *de novo* enhancers (58%), IRF3 binding to C1 and C2 enhancers showed similar low frequency (~22%) (Figure 2.2B). These results suggest that IRF3's role in *de novo* enhancer formation may be indirect, *via* IFNβ production that activates ISGF3.

To further understand the role of IRF3 in formation of enhancers, we investigated ISGF3 activity in *Irf3*$^{-/-}$ BMDMs by immunoblots of nuclear extracts. We observed a deficiency in the activation of ISGF3 subunits STAT1 and STAT2 in response to LPS (Figure 2.2C), in agreement with IRF3's role in IFNβ production (Sakaguchi et al. 2003). Thus, deficiencies in enhancer formation observed in IRF3 knockout cells may be due to defects in ISGF3 activation. Thus, we rescued ISGF3 activation in *Irf3*$^{-/-}$ BMDMs by co-stimulating LPS-treated cells with 0.3 or 10 U/mL of IFNβ at 1 hour of the LPS stimulation timecourse (Figure 2.2C). Co-stimulation with 10 U/mL IFNβ showed similar nuclear pSTAT1 and pSTAT2 levels as LPS-treated WT cells. We therefore performed H3K4me1 ChIP-seq in *Irf3*$^{-/-}$ BMDMs stimulated with LPS or LPS+IFNβ (Figure 2.2D and 2.2E). We observed a 60% increase in H3K4me1 signal (on average) in the IRF-associated enhancers with the addition of IFNβ (p<0.001) (Figure 2.2D), while there was no statistical difference in the NFκB-associated enhancers (Figure 2.2E). These data indicate that

ISGF3 plays a greater role in the formation of enhancers, but there are some regions that might still require IRF3.

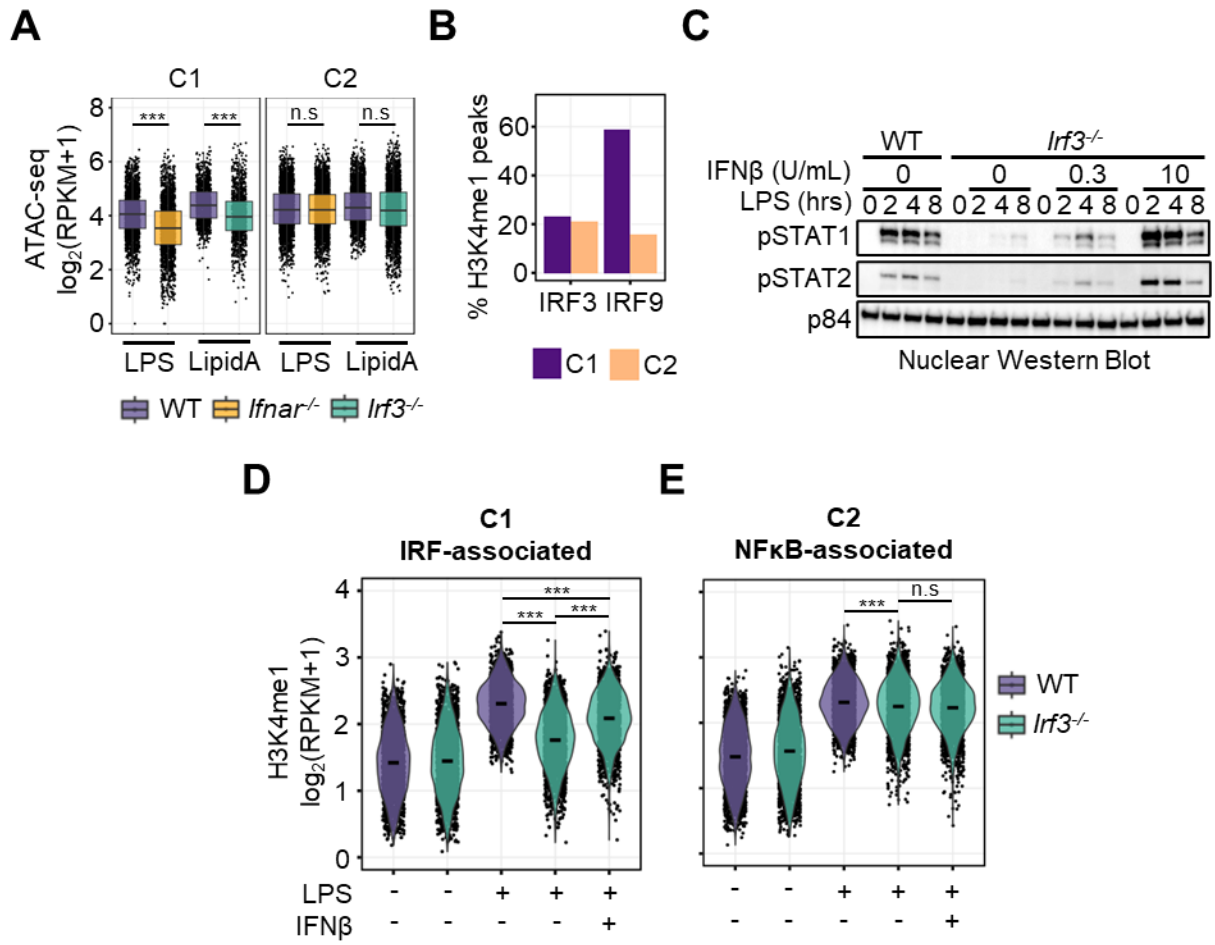

Figure 2.2. IFNβ rescues ISGF3 activity in *Irf3*$^{-/-}$ BMDMs. (A) Boxplots of $\log_2$ RPKM counts of ATAC-seq at C1 or C2 enhancer locations in WT, *Ifnar*$^{-/-}$, or *Irf3*$^{-/-}$ BMDMs treated with 100 ng/mL of LPS or Lipid A for 2 hours. (B) Percentage of H3K4me1 peaks with IRF3 (GSE67357) or IRF9 (GSE115435) binding to C1 or C2 enhancers. (C) Immunoblots of pSTAT1, pSTAT2, and loading control p84 using nuclear extracts from WT and *Irf3*$^{-/-}$ BMDMs stimulated with LPS with the indicated addition of IFNβ at the one-hour timepoint. (D-E) Violin plots of $\log_2$ RPKM counts of H3K4me1 ChIP-seq for C1 or C2 enhancers. Statistical significance was determined by Wilcoxon rank-sum test. p-values: <0.05 *, <0.001 **, <0.0001 ***.

2.3. ISGF3 is required but not sufficient to form most IRF-associated enhancers

To distinguish between *de novo* enhancers on the basis of their IRF3 involvement, we further classified the C1 enhancers into 3 different groups based on wildtype to *Irf3*$^{-/-}$ fold change differences (WT/*Irf3*$^{-/-}$) ; C1.1 enhancers were deficient in *Irf3*$^{-/-}$ BMDMs and were not rescued by IFNβ (LFC >0.5 in LPS and LFC>0.5 in LPS+IFNβ); C1.2 enhancers were rescued by IFNβ (LFC >0.5 in LPS and LFC < 0.5 LPS+IFNβ); and C1.3 enhancers showed only a moderate decrease in *Irf3*$^{-/-}$ BMDMs (LFC <0.5 in LPS) (Figure 2.3A). Of the 1090 *de novo* enhancers substantially affected by IRF3-deficiency, we found that 870 were rescued by the addition of IFNβ (C1.2), while only 220 locations remained deficient in enhancer formation even in the presence of ISGF3 activation (C1.1) (Figure 2.3B). To determine if these regions were defective in chromatin opening, we examined ATAC-seq data from WT and *Ifnar*$^{-/-}$ BMDMs (LPS-treated) and WT and *Irf3*$^{-/-}$ BMDMs (Lipid A-treated). We observed that IRF3-regulated *de novo* enhancers (C1.1) were more defective in chromatin opening in *Irf3*$^{-/-}$ BMDMs than those that were rescued by IFNβ-induced ISGF3 (Figure 2.3C). Furthermore, IRF3 ChIP-seq levels were significantly higher in the IRF3-dependent enhancers (C1.1) than in C1.2 or C1.3 enhancers (Figure 2.3D).

Since the majority of locations seemed to be rescued by ISGF3, we then interrogated whether ISGF3 alone is sufficient to trigger the formation of these enhancers. We stimulated WT macrophages with IFNβ, which activates ISGF3 but not IRF3. Remarkably, IFNβ treatment induced any of the C1 subcategories of enhancers less than 0.2 $\log_2$ RPKM whereas LPS generally induced them more than 1.0 $\log_2$ RPKM (Figure 2.3E). These results suggested that ISGF3 requires an additional LPS-induced co-factor to produce *de novo* enhancers.

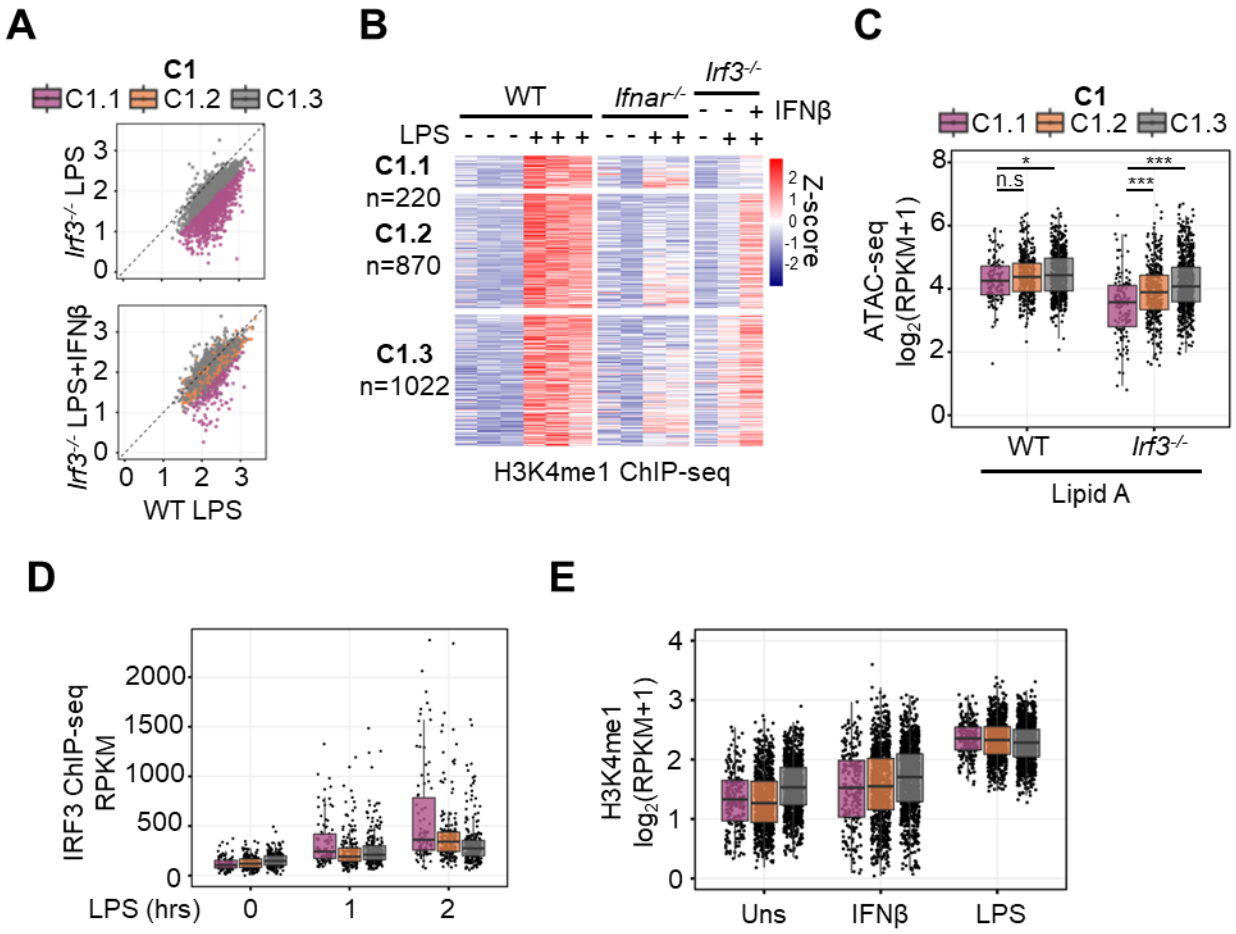

Figure 2.3. ISGF3 is required but not sufficient to form most IRF-associated enhancers.

(A) Scatterplots indicating $\log_2$ RPKM H3K4me1 ChIP-seq counts of C1 locations on LPS-stimulated WT BMDMs (*x*-axis) versus *Irf3*$^{-/-}$ (*y*-axis) (top) or additionally supplemented with IFNβ (bottom). Colors indicate three different groups determined by fold change cutoff thresholds of WT compared to *Irf3*$^{-/-}$ (WT/*Irf3*$^{-/-}$); C1.1 (purple) LFC >0.5 in LPS and LFC>0.5 in LPS+IFNβ, C1.2 (orange) LFC >0.5 in LPS and LFC < 0.5 LPS+IFNβ, C1.3 (grey) LFC <0.5 in LPS. (B) Heatmap of z-scored H3K4me1 ChIP-seq signal in the C1 locations (n = 2112) on LPS-stimulated WT, *Ifnar*$^{-/-}$, or *Irf3*$^{-/-}$ BMDMs or additionally supplemented with IFNβ. (C) Boxplots of $\log_2$ RPKM counts of ATAC-seq signal for C1.1, C1.2, or C1.3 enhancer locations in Lipid A stimulated WT or *Irf3*$^{-/-}$ BMDMs. (D) Boxplots of $\log_2$ RPKM counts of IRF3 ChIP-seq (GSE67357) for Lipid A-treated BMDMs at the C1.1, C1.2, or C1.3 enhancer locations. (E)

Boxplots of $\log_2$ RPKM counts of H3K4me1 ChIP-seq for WT BMDMs unstimulated, IFNβ stimulated (1 U/mL) or LPS (100 ng/mL) stimulated.

2.4 Formation of de novo *IRF-associated enhancers requires the combinatorial activity of IRF1 and ISGF3*

We hypothesized that another IRF may work in concert with ISGF3 to produce *de novo* enhancers. IRF1 has primarily been studied in context of the type II interferon (IFNγ) response (Ostuni et al. 2013; Abou El Hassan et al. 2017; Kang et al. 2019) as its expression is induced through the STAT1 homodimer GAF (Pine 1997). While type I interferon-activated ISGF3 does not induce IRF1 expression, LPS-activated NFκB does (Figure 1.5). To determine whether IRF1 plays a role in LPS-induced *de novo* enhancer formation, we stimulated BMDMs of *Irf1*$^{-/-}$ mice with LPS and performed H3K4me1 ChIP-seq. Principal component analysis (PCA) on the previously identified set of 4800 LPS-induced enhancers showed that *Irf1*$^{-/-}$ BMDMs are similar to *Irf3*$^{-/-}$ and *Ifnar*$^{-/-}$ BMDMs (Figure 2.4A). Unlike *Ifnar*$^{-/-}$ and *Irf3*$^{-/-}$ BMDMs, *Irf1*$^{-/-}$ BMDMs still retain LPS-induced ISGF3 activity (Figure 2.4B), suggesting that, in addition to ISGF3, IRF1 also plays a critical role in *de novo* enhancer formation. To explore the relative contribution of these two factors, we used knockout data to compare to wildtype (WT/KO) and classified the LPS-induced enhancers into those that are ISGF3-dominant (Group 1; LFC>0.5, FDR<0.05 in *Ifnar*$^{-/-}$), IRF1-dominant (Group 2; LFC>0.5, FDR<0.05 in *Irf1*$^{-/-}$), ISGF3- and IRF1- fully dependent (Group 3; LFC>0.5, FDR<0.05 in both *Irf1*$^{-/-}$ and *Ifnar*$^{-/-}$), or ISGF3- and IRF1-independent as a control group (Group 4; FDR>0.8) (Figure 2.4C-D). While the WT H3K4me1 RPKM values averaged 2.3-2.4 log2 RPKM in each of the four groups, mean RPKM values in *Ifnar*$^{-/-}$ were 1.4 and 1.5 in Groups 1 and 3, respectively, and in *Irf1*$^{-/-}$ were 1.5 in both Groups 2 and 3 (p<0.001 for all comparisons) (Figure 2.4D). In the control group, no effect was observed in either knockout (Figure 2.4C and 2.4D). The IRF1/ISGF3-dependent *de novo* enhancers were largely distinct from the IRF3-dependent *de novo* enhancers, as only 9% of G1, 12% of G2, or 6% of G3 enhancer regions overlapped with the enhancer locations within cluster C1.1 (Figure 2.3A-C).

TF motif enrichment analysis revealed single nucleotide differences in the connecting region between the half-sites: CT in Groups 1 and 3 *vs.* GT in Group 2. In addition, the 3' end of the motif in Group 1 was shorter (Figure 2.4E). These subtle differences may partially contribute to differential IRF requirements (Csumita et al. 2020; Näf et al. 1991; Ourthiague et al. 2015). Therefore, we examined publicly available IRF1 and IRF9 ChIP-seq datasets of BMDMs stimulated with LPS or IFNβ, respectively (Mancino et al. 2015; Platanitis et al. 2019). We determined the IRF1 and IRF9 binding locations and the overlap with the *de novo* enhancer locations (Figure 2.4F and 2.4G). We found that 76% of the ISGF3-dominant *de novo* enhancers had IRF1 binding while 95% of the IRF1-dominant *de novo* enhancers had IRF1 binding. In contrast 75% of the ISGF3 dominant peaks and 67% of the IRF1-dominant enhancers had IRF9 binding. We observed similar strong binding of IRF1 and IRF9 in the IRF1 and ISGF3 dependent group (>85%) and less binding to locations within the IRF1 and ISGF3 independent group (Figure 2.4F and 2.4G). These results suggest that while both IRF1 and ISGF3 are involved in the formation of IRF-associated *de novo* enhancers, subtly distinct binding preferences to ISRE motif variants may contribute to the observed differential genetic requirements of IRF1 and ISGF3.

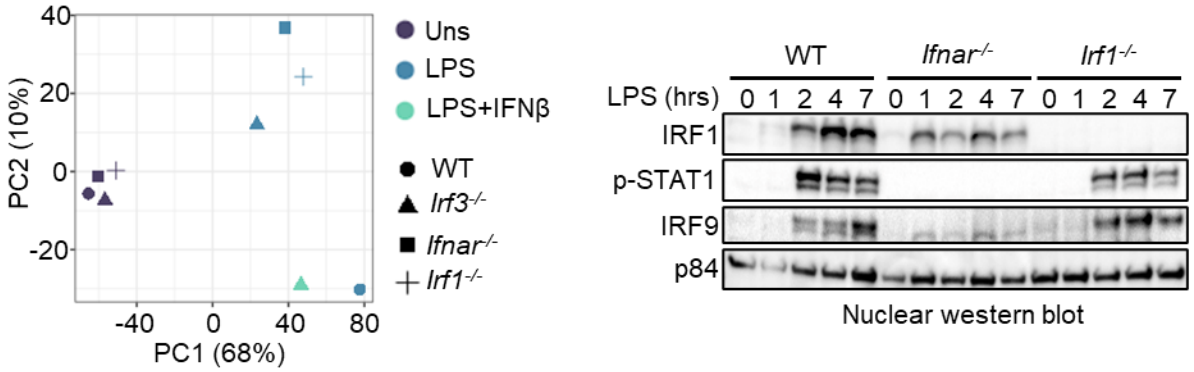

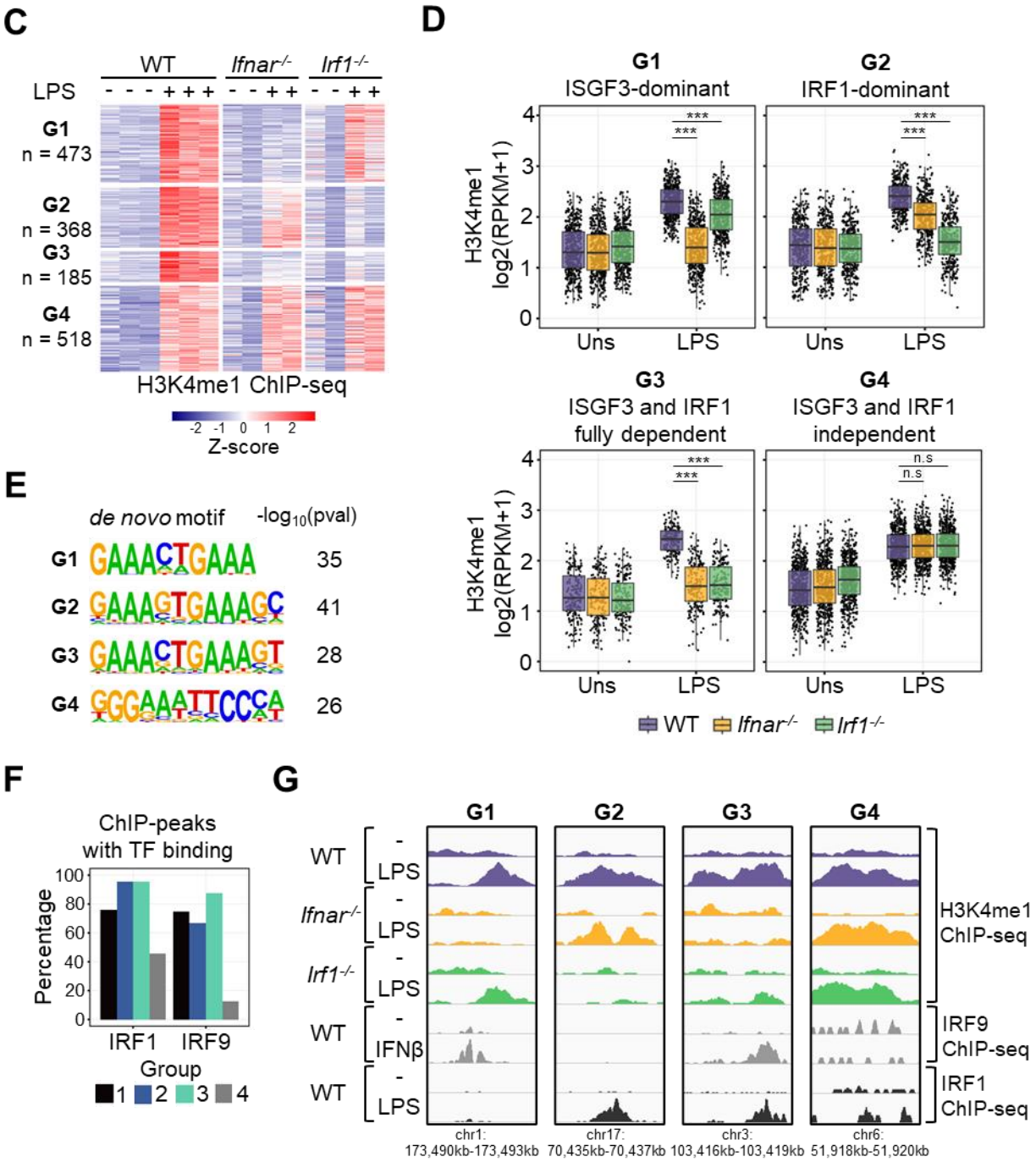

Figure 2.4. IRF-associated *de novo* enhancer formation requires both IRF1 and ISGF3. (A) PCA plot of H3K4me1 ChIP-seq dynamics among WT, *Irf3*$^{-/-}$, *Ifnar*$^{-/-}$, and *Irf1*$^{-/-}$ BMDMs with the indicated stimulus. (B) Immunoblots of IRF1, p-STAT1, IRF9 and loading control p84 in WT, *Ifnar*$^{-/-}$, or *Irf1*$^{-/-}$ BMDMs stimulated with LPS. (C) Heatmap of z-scored H3K4me1 ChIP-seq data

after 8 hours of LPS stimulation of WT, *Ifnar*$^{-/-}$, or *Irf1*$^{-/-}$ BMDMs. The 4800 LPS-induced enhancers (2.1B; C1 and C2) were filtered into those that are IFNAR-dependent (Group 1; LFC>0.5, FDR<0.05 WT/*Ifnar*$^{-/-}$), IRF1-dependent (Group 2; LFC>0.5, FDR<0.05 WT/*Irf1*$^{-/-}$), dependent on both factors (Group 3; LFC>0.5, FDR<0.01 WT/*Ifnar*$^{-/-}$ and WT/*Irf1*$^{-/-}$), or independent of both factors (Group 4; FDR>0.8 in WT/*Ifnar*$^{-/-}$ and WT/*Irf1*$^{-/-}$), for a total of 1544 genomic locations. (D) Boxplots of $\log_2$ RPKM counts of H3K4me1 ChIP-seq for the groups determined in (C). (E) *De novo* transcription factor motif analysis of each group in Figure B with corresponding adjusted p-values. (F) Percentage of H3K4me1 peaks overlapping with binding events of IRF1 (LPS stimulation) (GSE56123) or IRF9 (IFNβ stimulation) (GSE115435). (G) H3K4me1 genome browser tracks of representative *de novo* enhancer regions of G1, G2, G3, and G4. Statistical significance was determined by Wilcoxon rank-sum test. p-values are indicated: <0.05 *, <0.001 **, <0.0001 ***.

2.5 IRF1 and ISGF3 have sequential roles in the formation of IRF-associated de novo *enhancers*

To assess the mechanistic roles of IRF1 and ISGF3 in opening chromatin, we performed ATAC-seq on BMDMs stimulated with 100 ng/mL LPS for 0, 1, 2, and 4 hours. We then found the overlap between the ATAC-seq peaks and the LPS *de novo* enhancer regions. Using the same four groups determined in Figure 3, we observed similar overall trends of IRF factor dependency in chromatin opening (Figure 2.5A-C). Intriguingly, however, upon close examination of individual time points, we observed that the deficiency of chromatin opening in *Ifnar*$^{-/-}$ BMDMs was not significant until 2 hours, while *Irf1*$^{-/-}$ BMDMs diverged from WT within 1 hour of stimulation (Figures 2.5B-D). The temporal specificity in *Irf1 vs. Ifnar* requirement was more prominent for the highly IRF1-dependent groups (Group 2 and 3) than the ISGF3 dominant group (Group 1).

Next, we quantitatively compared the relationship between chromatin opening by ATAC-seq and formation of *de novo* enhancers by ChIP-seq (Figure 2.5E). As a reference point of comparison, we calculated the fraction of H3K4me1 signal loss in *Ifnar*$^{-/-}$ or *Irf1*$^{-/-}$ relative to WT at eight hours for each location. We also calculated the fraction of ATAC-seq signal loss in *Ifnar*$^{-/-}$ or *Irf1*$^{-/-}$ relative to WT for each location at all three timepoints. We then used spearman coefficients to determine whether loss of ATAC-seq signal correlated with loss of ChIP-seq signal. We found that for both genotypes, at the 4h timepoint losses of ATAC-seq signal correlated with losses of ChIP-seq signal, with $\rho > 0.4$ for all groups of locations (Figure 2.5E). However, at early timepoints, in *Ifnar*$^{-/-}$ BMDMs the ATAC signal did not mirror the loss of the later ChIP-seq signal; this was especially evident at one hour, where the correlation coefficient was near zero for all groups of locations (Figure 2.5E). In contrast, the loss of ATAC signal in *Irf1*$^{-/-}$ is correlated with the loss of the subsequent ChIP-seq signal even at the 1h timepoint. These results suggested that IRF1 plays a critical role in the initial steps of opening chromatin

while ISGF3 is important in subsequent steps with both being required for *de novo* enhancer formation.

To characterize the basal chromatin state, we investigated available BMDM datasets and found that groups G2 and G3, which are highly IRF1-dependent, show lower ATAC-signals as well as less PU.1 and RNAPol II binding than group G1, which contains locations that have a less strict IRF1 requirement (Figure 2.5F) (Ostuni et al. 2013). Taken together, these results suggest that IRF1 plays a particularly critical role at locations where chromatin is tightly compacted and shows lower factor binding associated with enhancer priming and basal activity.

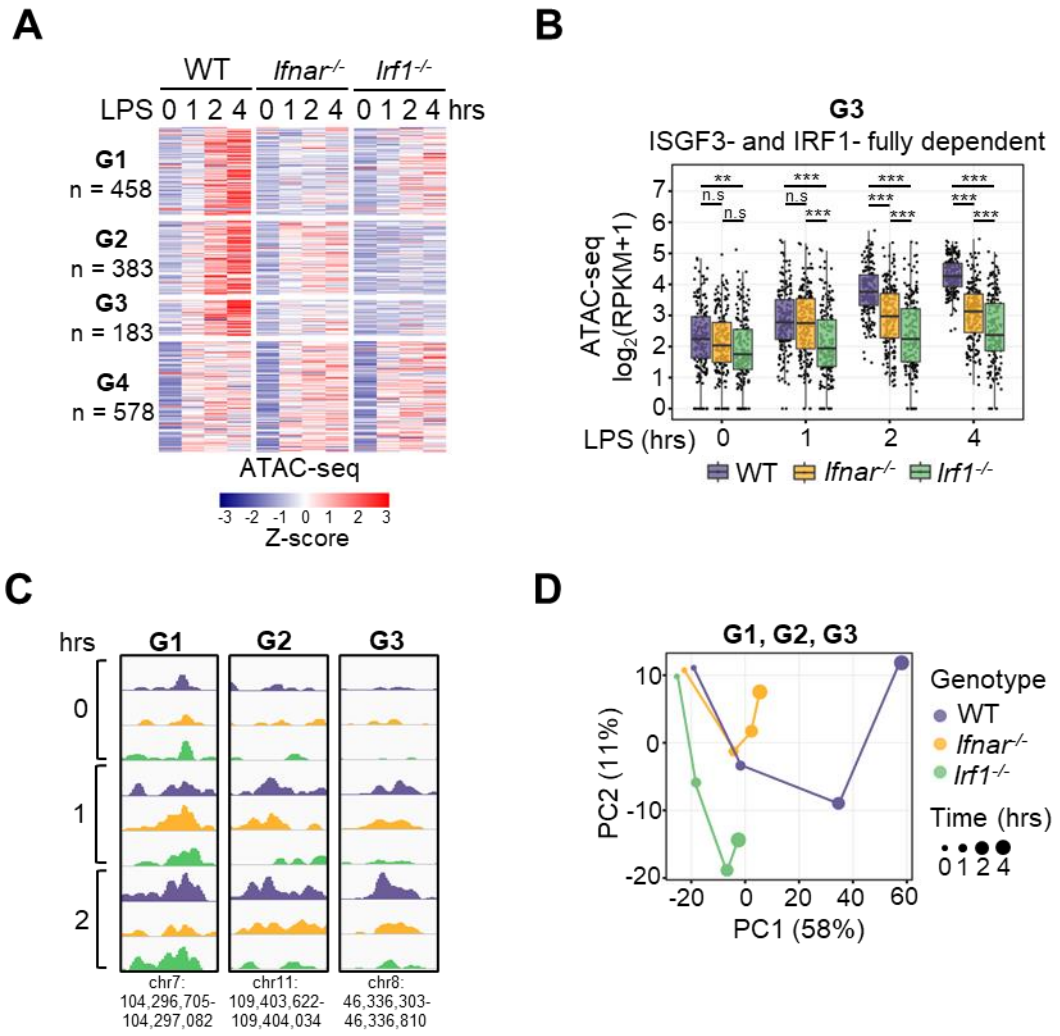

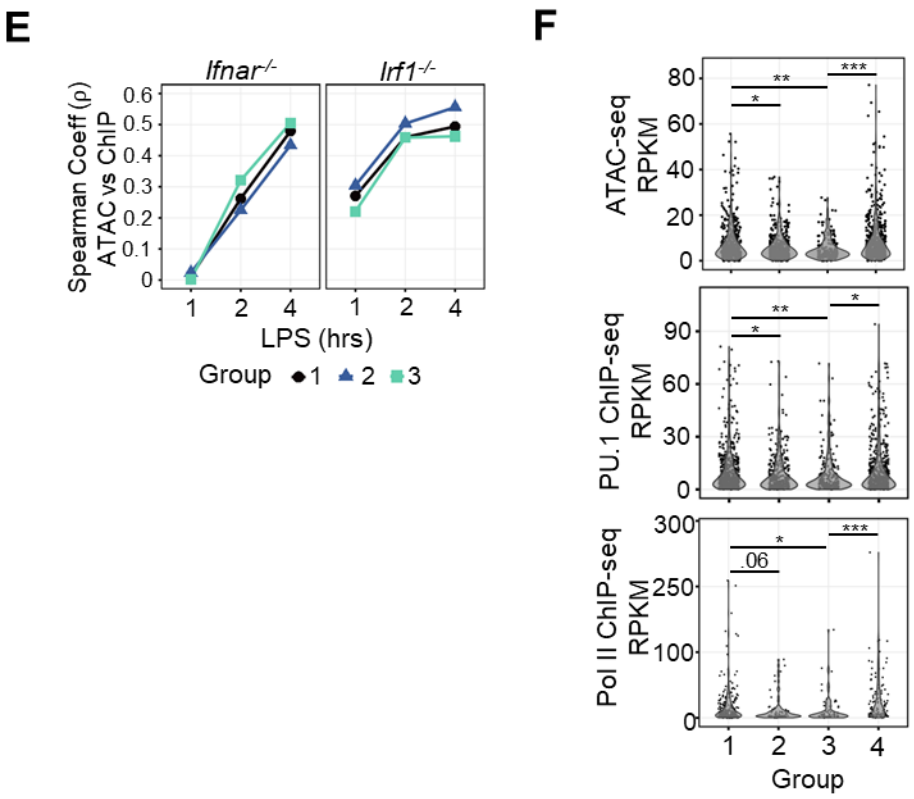

Figure 2.5. Differential temporal roles of IRF1 and ISGF3 in opening chromatin at IRF-associated enhancer locations. (A) Heatmap of z-scored ATAC-seq signal from the peaks that overlap with *de novo* enhancer regions (Figure 2.4C) after LPS stimulation for the indicated times. (B) Boxplot of $\log_2$ RPKM counts of ATAC-seq signal in group 3 locations, which are dependent on both ISGF3 and IRF1. No deficiency is seen in *Ifnar*$^{-/-}$ at 1h timepoint. (C) Genome browser tracks of representative locations for groups 1, 2, and 3 for WT, *Ifnar*$^{-/-}$ and *Irf1*$^{-/-}$ BMDMs. (D) PCA plots of ATAC-seq groups 1, 2, and 3, at the indicated timepoints and genotypes. (E) Spearman correlation analysis of knockout H3K4me1 signal as a percentage of WT and knockout ATAC-seq signal as a percentage of WT. Loss of H4K4me1 signal in knockouts is generally mirrored by loss of ATAC-seq signal, but not at 1h timepoint for *Ifnar*$^{-/-}$. (F) Violin plots of RPKM counts of ATAC-seq, PU.1 ChIP-seq or RNA Pol II ChIP-seq (GSE38377) in the basal state at the four different groups. Statistical significance was determined by Wilcoxon rank-sum test. p-values are indicated: <0.05 *, <0.001 **, <0.0001 ***.

2.6. Molecular characteristics of IFNγ de novo *enhancers*

Having shown that IRF1 plays a critical role in chromatin remodeling downstream of LPS, we wondered whether IRF1 plays a similar role when induced by IFNγ through GAF. IFNγ-stimulation of macrophages leads to broad chromatin remodeling (Ostuni et al. 2013; Cheng et al. 2021; Platanitis et al. 2022), but it is not clear which SDTFs are responsible. Previous studies have suggested, by ChIP-seq analyses, that ISGF3 components IRF9 and STAT2 aid IFNγ-induced transcriptional gene activation (Platanitis et al. 2019) but not chromatin opening (Platanitis et al. 2022). To directly assess whether ISGF3 activity is induced in BMDMs upon IFNγ stimulation, we performed electrophoretic mobility shift assay (EMSA) with probes for GAF and ISGF3. Our data reveals that while GAF is activated at the lowest dose of IFNγ (3ng/mL), but even the highest dose (100ng/mL) did not activate ISGF3 (Figure 2.6A). In addition, nuclear western blots did not detect activation of p-STAT2 upon IFNγ stimulation, while p-STAT1 and IRF1 were highly induced (Figure 2.6B).

In the absence of activated ISGF3, we hypothesized that IRF1 may be a critical factor in IFNγ-induced *de novo* enhancer formation. Therefore, we performed H3K4me1 ChIP-seq on IFNγ-stimulated (100 ng/mL) WT and *Irf1*$^{-/-}$ BMDMs. We identified 2231 *de novo* enhancer regions by applying a cut-off of FDR<0.01 log2FC>0.5 on duplicate data in wild type cells, and 1820 IFNγ *de novo* enhancers that were IRF1-dependent (FDR<0.01 log2FC>0.5), while 411 appeared to be IRF1-independent (Figure 2.6C). Indeed, motif enrichment analysis revealed that the top motif for IRF1-dependent enhancers is “IRF1” and for IRF1-independent enhancers is “STAT1” (Figure 2.6C). Similar to the LPS-induced enhancers, we also observed that the basal chromatin state in WT BMDMs is less accessible in the IRF1-dependent group than the IRF1-independent group (Figure 2.5D). Further, analysis of H3K27ac and PU.1 ChIP-seq data from BMDMs (Ostuni et al. 2013) revealed that in basal conditions the genomic regions of IRF1-dependent *de novo* enhancers have lower H3K27ac and PU.1 binding levels than the IRF1-

independent enhancers (Figure 2.6E-F). These results suggest that GAF can remodel chromatin without IRF1 requirement only at a minority of locations where the chromatin state is less compacted and are pre-bound by PU.1; however, IRF1 is required for the majority of IFNγ *de novo* enhancers.

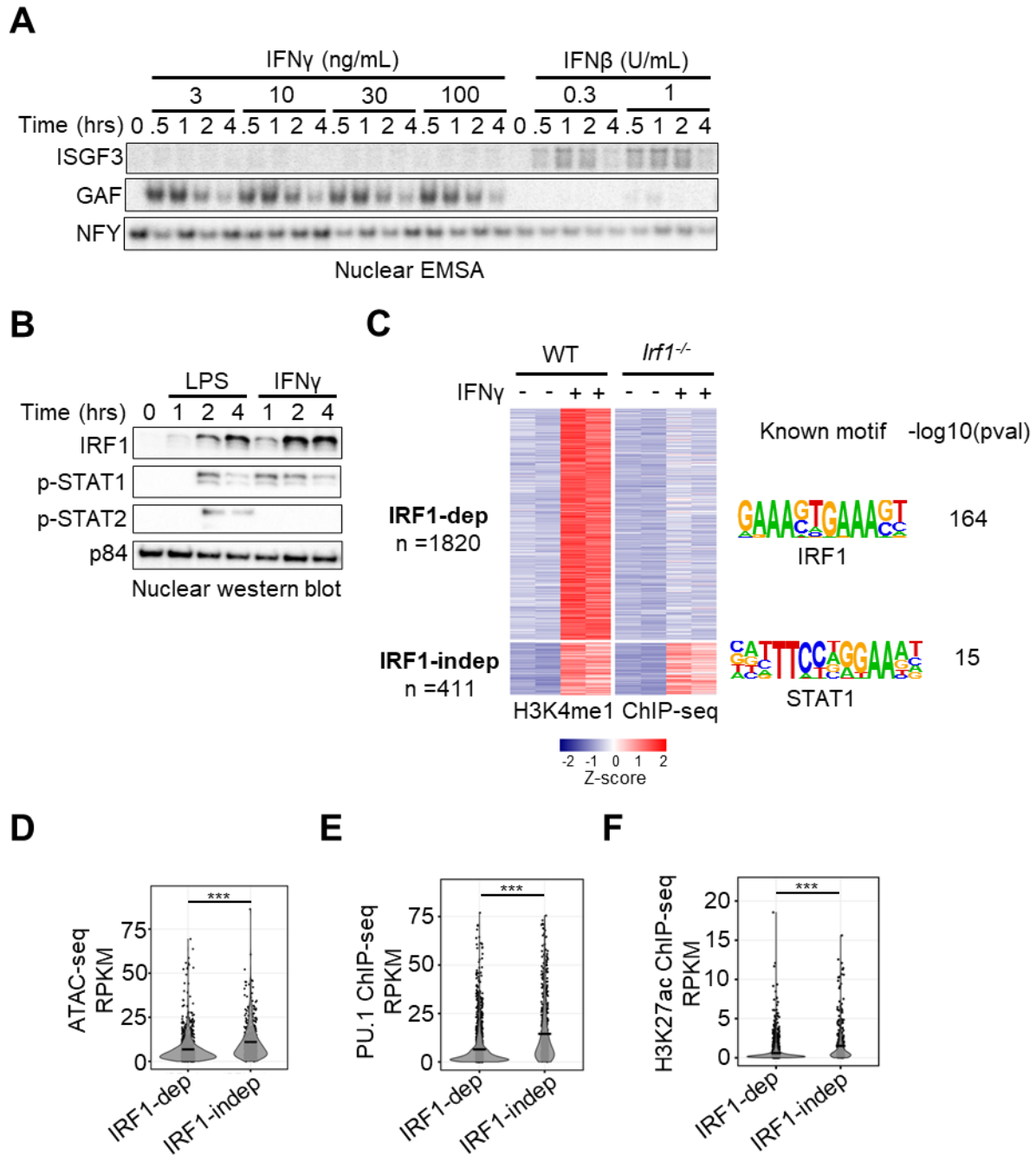

Figure 2.6. Chromatin remodeling of IFNγ-induced enhancers is dependent on IRF1. (A) ISGF3, GAF, and NFY activities revealed by an electrophoretic mobility shift assay (EMSA) on nuclear extracts of WT BMDMs stimulated with various doses of IFNγ. Data are representative of n >3 independent experiments. (B) IRF1, p-STAT1, p-STAT2, IRF9, and p84 nuclear abundance revealed by nuclear western blot in WT BMDMs stimulated with LPS (100ng/mL), IFNγ (100ng/mL), or IFNβ (1U/mL) at the indicated timepoints. (C) Heatmap of z-scored H3K4me1 ChIP-seq data showing 2231 regions induced after 8 hours of IFNγ (100ng/mL) stimulation (LFC>0.5, FDR<0.01). IRF1-dependent and independent clusters determined by FDR<0.05, LFC>0.5 compared to WT. Top hit of known transcription factor motif enrichment for each group are shown. (D-F) Violin plots of RPKM counts at the basal state of (D) ATAC-seq (E) PU.1 ChIP-seq or (F) H3K27ac ChIP-seq in the IFNγ-induced enhancer locations (GSE38377). Statistical significance was determined by Wilcoxon rank-sum test. p-values are indicated: <0.05 *, <0.001 **, <0.0001 ***.

2.7 IRF1 may function in concert with ISGF3 or GAF to produce de novo *enhancers*

We asked whether IRF1 cooperates with ISGF3 (when induced by LPS) or GAF (when induced by IFNγ) at the same enhancer locations. Of the 1820 IFNγ-induced IRF1-dependent *de novo* enhancers and the 1026 LPS-induced IRF1/ISGF3-dependent *de novo* enhancers, 459 LPS-induced *de novo* enhancers (20%) did not pass the significance threshold with IFNy (Figure 2.7A; LPS-specific), while 1258 H3K4me1 regions (55%) were significantly induced by IFNy but did not pass the significance threshold in the LPS condition (Figure 2.7A; IFNy-specific). Of the 567 locations (25%) induced by both LPS and IFNy, *de novo* motif analysis revealed an IRF1 binding sequence consensus (Figure 2.7B), which we had also identified in the ISGF3-and-IRF1-dependent G3 group (Figure 2.4E). The formation of these *de novo* enhancers that are common to LPS or IFNy was highly dependent on IRF1, however a stronger deficiency was observed by IFNy (Figure 2.7C). These data suggest that ISGF3 activation by LPS might have stronger *de novo* enhancer formation properties than GAF induction by IFNy, or that IRF1 is required to bind directly with GAF.

Using publicly available ChIP-seq data (Langlais et al. 2016; Ng et al. 2011; Platanitis et al. 2019), we found that out of the 567 *de novo* enhancers 354 show STAT1 (GAF) binding in response to IFNy and 452 show IRF9 (ISGF3) binding in response to LPS, with 268 showing binding by all three factors IRF1, IRF9 (ISGF3) and STAT1 (GAF) in the respective stimulus conditions (Figure 2.7D-E). Despite the high false negative rate of transcription factor ChIP-seq results, these observations provide physical binding data confirmation of the genetic results, that IRF1 may cooperate with GAF to form IFNγ-induced *de novo* enhancers and cooperate with ISGF3 to form LPS-induced *de novo* enhancers.

To further investigate the cooperativity mechanism of GAF-IRF1, we classified the IFNγ-specific enhancers based on IRF1 or STAT1 binding. Among the 1258 IFNγ-specific enhancers, 260 showed IRF1 binding only (21%), 114 showed STAT1 binding only (9%), 291 showed both

IRF1 and STAT1 binding (23%), and 593 showed no binding by either (47%). 64% of IRF1-only binding events contained IRF motifs, while 61% of STAT1-only binding events featured a GAS motif, indicating that STAT1 and IRF1 preferably bind to their respective cognate motifs but can also interact with non-consensus sequences (Figure 2.7F). Within the regions that were bound by both IRF1 and STAT1, 41% contained both IRF and GAS motifs (Figure 2.7F). To further gain insights into the functional dynamics of these complexes activating *de novo* enhancers, we analyzed H3K27ac levels in these groups. Upon IFNγ stimulation, locations with STAT1 binding had significantly higher levels of H3K27ac signal, with the highest levels observed where IRF1 and STAT1 both bind (p<0.001) (Figure 2.7G). At the basal state, only the locations that had both IRF1 and GAF binding exhibited significantly higher levels of H3K27ac (p<0.001) (Figure 2.7G). Collectively, these results suggest cooperativity between IRF1 and STAT1 to produce active *de novo* enhancers.

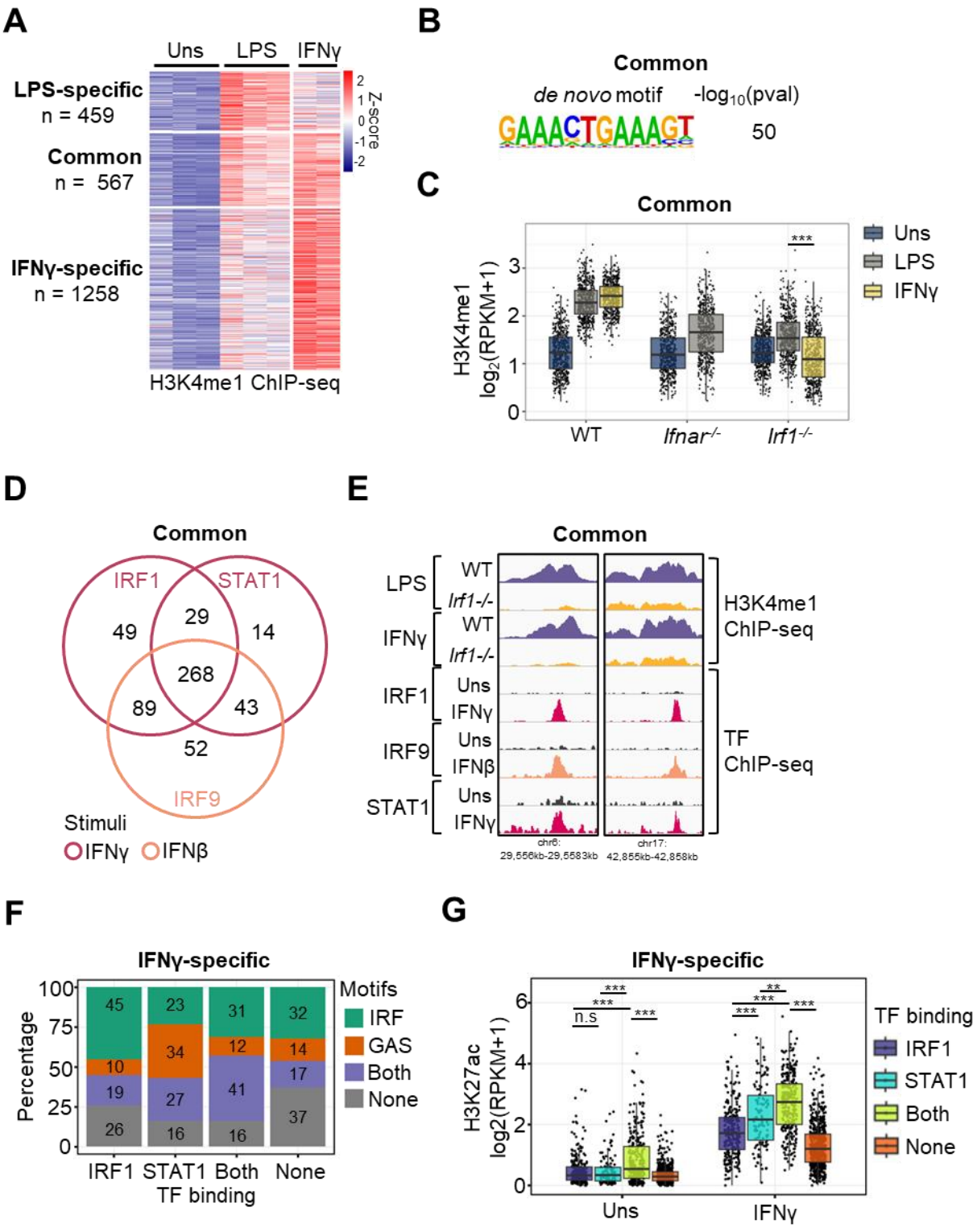

Figure 2.7. IRF1 cooperates with ISGF3 or GAF to trigger active *de novo* enhancer formation. (A) Heatmap of z-scored H3K4me1 ChIP-seq data showing 2279 regions induced

by LPS or IFNγ stimulation. Groups were defined as the LPS inducible regions (LFC>0.5, FDR<0.05) or IFNγ inducible regions (LFC>0.5, FDR<0.01) that passed the threshold of FDR<0.05 and LFC>0.5 the *Ifnar*$^{-/-}$ (LPS) or *Irf1*$^{-/-}$ (LPS and IFNγ) in LPS only (LPS-specific) IFNγ only (IFNγ-specific) or in both (common). (B) Top hit from *de novo* transcription factor motif analysis of the "common" group and corresponding p-value. (C) Boxplot of $\log_2$ RPKM H3K4me1 signals for "common" group in WT, *Ifnar*$^{-/-}$, or *Irf1*$^{-/-}$ BMDMs. (D) Venn diagram of IRF1 (IFNγ stimulation) (GSE77886), STAT1 (IFNγ stimulation) (GSE115435, .6.0) or IRF9 (IFNβ stimulation) (GSE115435) ChIP-seq peaks in the "common" *de novo* enhancer locations. (E) Genomic browser tracks of representative regions of the "common" *de novo* enhancers. (F) Bar graphs indicating percentage of "IFNγ-specific" enhancers associated with indicated motifs. "IFNγ-specific" enhancers were grouped based on IRF1 or STAT1 binding. (G) Boxplot of $\log_2$ RPKM H3K27ac signals at basal or after 4 hours of IFNγ (100 ng/mL) stimulation (GSE38377) at the "IFNγ-specific" locations. Colors indicate *de novo* enhancers with the indicated transcription factor binding. Statistical significance was determined by Wilcoxon rank-sum test. p-values are indicated: <0.05 *, <0.001 **, <0.0001 ***.

.

2.8 Potentiation of genes nearby enhancers by IFNγ training is dependent on IRF1

Next, we examined how IRF1-dependent enhancers alter macrophage transcriptional responses to subsequent stimulation. We stimulated WT BMDMs with IFNγ (100 ng/mL) for 8 hours, removed the stimulus, and let the cells rest for a total of 72 hours after primary stimulation. We then challenged these cells with LPS (0.1 ng/mL) for 0, 1.5, or 3 hours and collected samples for RNA-seq (Figure 2.8A). To assess the effect of IFNγ training in the LPS response, we first identified LPS-inducible genes by applying a threshold of LFC >0.5 after LPS treatment for at least one timepoint in PBS or IFNγ-trained conditions. For the resulting 1337 genes, we calculated the effect by IFNγ at the three-hour timepoint when compared to the PBS control and divided these fold changes into 10 bins (Figure 2.8B). In general, bins 1-5 were enriched for terms related to metabolic and growth processes, while bin 6 and higher were enriched for “Response to external biotic stimulus”, or “response to other organism” (Figure 2.8C). Interestingly, bin 10 had the highest enrichment of GO terms, and “Response to interferon-beta” was statistically significant only in this group. These results suggest that IFNγ tolerizes metabolic pathways while it potentiates inflammatory pathways and responses to innate immune challenges.

Next, we explored which genes were associated with the previously identified 1820 IRF-dependent IFNγ-induced *de novo* enhancers (Figure 2.8D). We found 791 genes within 100kb and clustered them based on their expression response to LPS by the k-means algorithm into three groups (I1-3) (Figure 2.8D). We found that Cluster 1 (I1) genes were not induced by LPS, and the enriched GO pathways were related to ‘growth response’ (Figure 2.8E). Cluster 2 (I2) genes showed diminished expression and were enriched for metabolic pathways. Cluster 3 (I3) genes showed potentiated LPS-responsiveness after IFNγ training. Intriguingly, the top matches for I3 were “response to external biotic stimulus,” “innate immune response,” and “cellular response to Type II IFN” (Figure 2.8E). We then tested IRF1 dependency, and we found that for

cluster 3 genes, the potentiation effect by IFNγ was abrogated by the loss of IRF1, though LPS-inducibility in untrained *Irf1*$^{-/-}$ BMDMs was retained (Figure 2.8F). When looking at the LPS-inducible genes of I3 (LFC > 0.5), the potentiation effect of IFNγ was reduced in the *Irf1*$^{-/-}$ for the vast majority of genes when viewed in a pairwise comparison of fold changes (p<0.001; Figure 2.8G). Genes in I3 included *Ifit3* and *Mx1*, as well as other ISGs (Figure 2.8H). These results suggest that IRF1-regulated enhancers potentiate the expression of a subset of IFNγ-responsive genes in a manner that is dependent on IRF1.

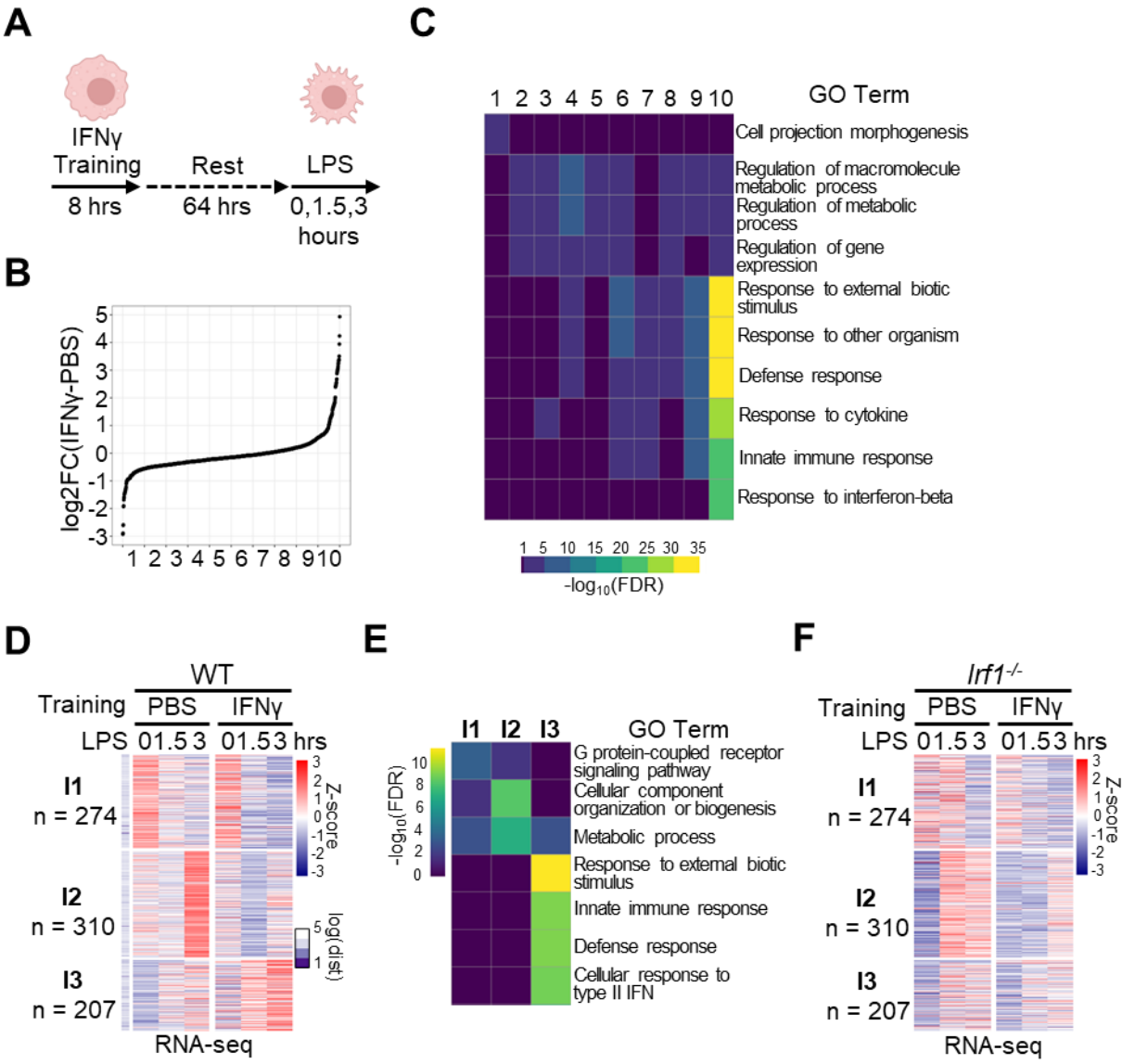

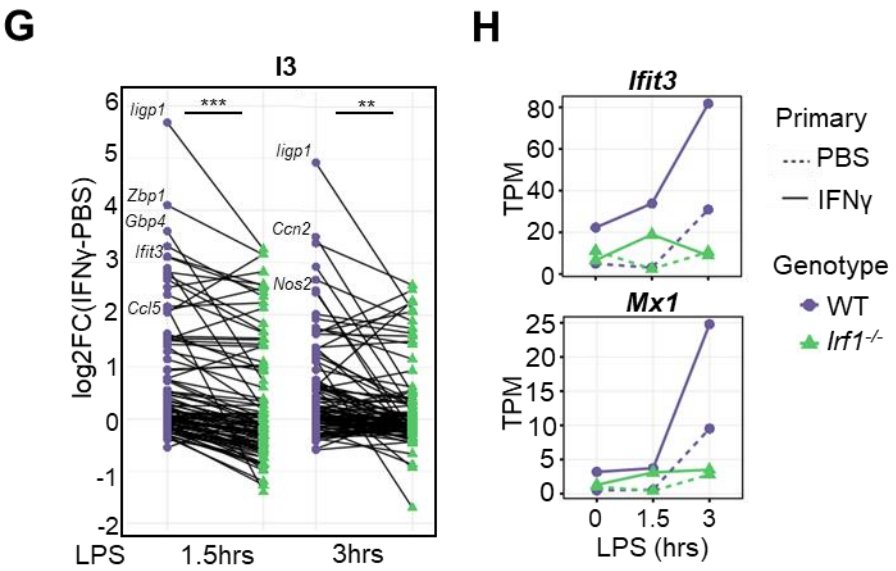

Figure 2.8. IFNγ-induced enhancers direct gene expression responses to a subsequent immune challenge. (A) Experimental scheme for induction of innate immune memory. BMDMs were stimulated with IFNy (100 ng/mL) for 8 hours, and after a 64-hour rest, challenged with LPS (0.1 ng/mL). (B) Distribution of IFNγ training LFC values at the 3-hour timepoint of the LPS challenge grouped into 10 equal bins. 1337 genes were selected as LPS-inducible (LFC >0.5) in at least one timepoint. (C) Heatmap showing top GO-term enrichments (biological process) for each bin. (D) Heatmap of z-scored RNA-seq signal of the nearest expressed genes to the IRF1-dependent IFNγ-induced *de novo* enhancers (Figure 2.6C; IRF1-dep). K-means clustering reveals three clusters (I1-3), where cluster 3 is potentiated by IFNγ training. (E) Heatmap showing most highly enriched GO terms for I1-3. (F) Heatmap of z-scored RNA-seq data in *Irf1*$^{-/-}$ BMDMs using same clusters as (D) shows IFNy potentiation loss of the I3 genes. (G) Paired dotplot showing LFC of IFNγ training on LPS-inducible (LFC > 0.5) cluster 3 (I3) genes, comparing WT (purple) and *Irf1*$^{-/-}$ (green) genotypes. (H) Lineplots of representative I3 genes showing effect of IFNγ training in WT and *Irf1*$^{-/-}$ BMDMs. Statistical significance was determined by Wilcoxon rank-sum test. p-values are indicated: <0.05 *, <0.001 **, <0.0001 ***.

2.9 IRF1- and ISGF3- dependent LPS-induced de novo *enhancers show potentiation of nearby genes*

It has been well established that LPS treatment leads to a state of tolerance, where cells respond to a second stimulation with lower inflammatory gene expression (Biswas and Lopez-Collazo 2009), but may maintain their ability to express genes related to tissue repair and antimicrobial effectors (Foster et al. 2007). In order to examine the significance of LPS-induced IRF-dependent enhancers, we trained macrophages with LPS (100ng/mL) for 8 hours, then challenged with LPS (0.1ng/mL) after 72 hours (Figure 2.9A). We found 1192 genes that were within 100kb of LPS-induced IRF-dependent enhancers. We filtered for the genes that were inducible in at least one timepoint of secondary LPS exposure either in PBS or LPS-trained macrophages (LFC > 0.5) and found 225 genes that clustered in two distinct clusters by the k-means algorithm (Figure 2.9B). Cluster 1 (L1) was characterized by tolerized genes that were enriched for GO terms such as “Regulation of gene expression” and “Regulation of cytokine production”. Interestingly, cluster 2 (L2) was characterized by potentiated genes that were strongly enriched for the GO terms “response to external biotic stimulus”, “response to other organism”, and “response to IFNβ” (Figure 2.9C). Additionally, we observed a decrease in potentiation of the L2 genes upon LPS training in both *Ifnar*$^{-/-}$ and *Irf1*$^{-/-}$ macrophages (Figure 2.9D). These results suggest that IRF-regulated enhancers potentiate the expression of a subset of LPS-responsive genes in a manner that is dependent on IRF1 and ISGF3.

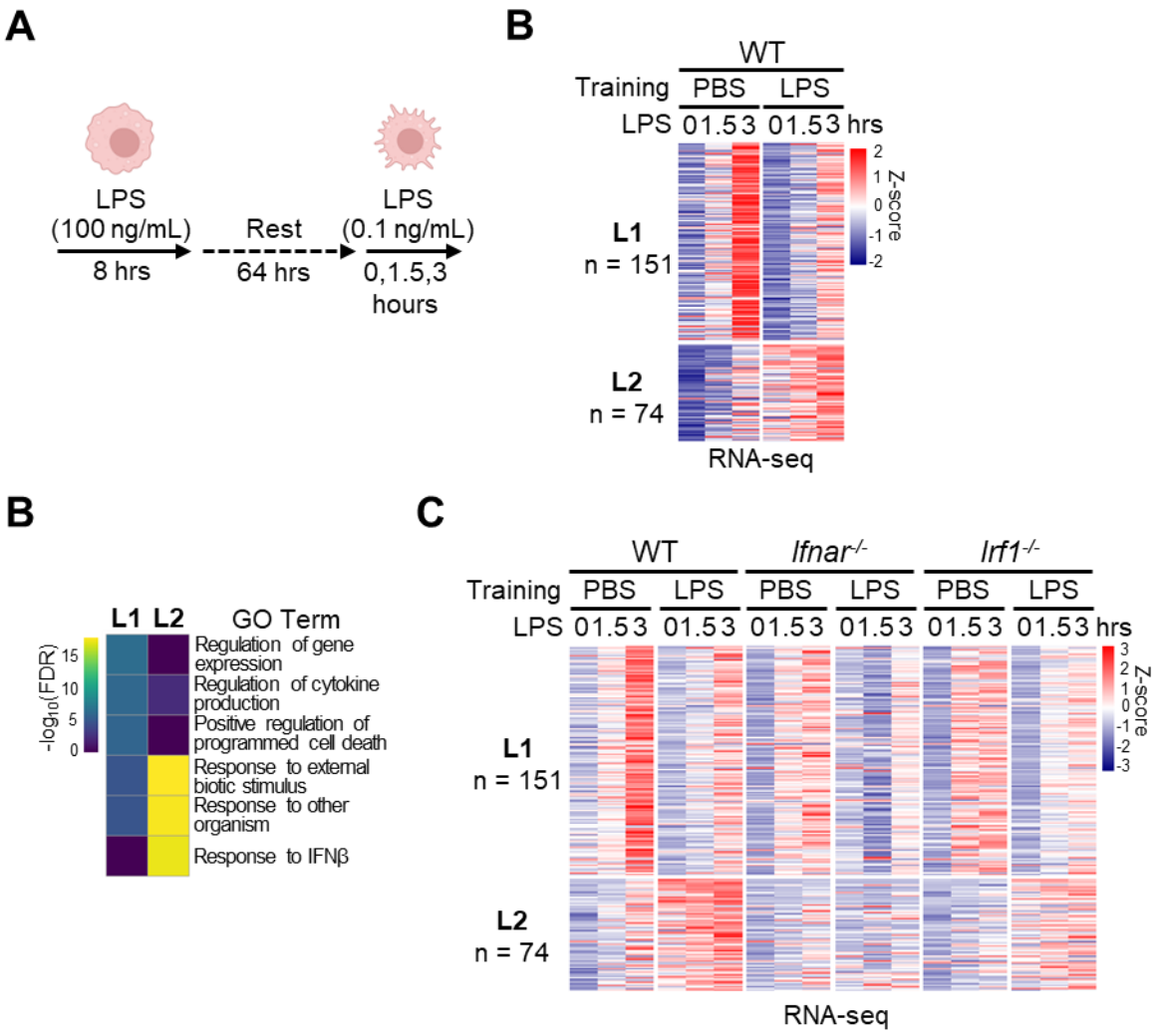

Figure 2.9. LPS-induced enhancers associate with potentiated gene expression responses to subsequent LPS exposure. (A) Experimental scheme for induction of innate immune memory. BMDMs were stimulated with LPS (100 ng/mL) for 8 hours, and after a 64-hour rest, challenged with LPS (0.1 ng/mL). (B) Heatmap of z-scored RNA-seq signal, showing genes within 100kb of enhancers that are LPS-inducible and IRF1 or IFNAR dependent (Fig. 2.4C; Groups 1-3). K-means clustering reveals two clusters, where cluster 2 (L2) is potentiated by LPS training. (C) Heatmap showing most highly enriched GO terms for the L1 and L2 as determined in (B). (D) Heatmap of z-scored RNA-seq data showing the same genes as in (B) in WT, *Ifnar*$^{-/-}$, and *Irf1*$^{-/-}$ BMDMs.

CHAPTER 3: DISCUSSION

CHAPTER 3: DISCUSSION

The evidence presented in this dissertation includes targeted gene knockouts, biochemical characterization of signaling pathways, and an exploration of factors binding to chromatin locations that acquire enhancer marks upon stimulation. Crucially, this investigation not only introduces novel datasets from key knockouts but also utilizes a broad range of datasets produced by several laboratories that paint a consistent narrative. This consistency across distinct cell cultures and experimental methodologies enhances the robustness and reliability of our conclusions.

Following pathogen infection, it is critical that the host develops a fast, fine-tuned, and regulated immune response. Innate immune memory in macrophages thus has developed as a mechanism to protect the host from further infections. This dissertation provides evidence of two distinct scenarios by which IRF1 functions as an epigenetic reprogramming in macrophages. Firstly, in infected macrophages, the combinatorial activation of IRF1 (*via* NFκB) and ISGF3 (*via* IFNβ signaling) will result in the epigenetic reprogramming of enhancers, influencing subsequent gene expression to immune challenges. Secondly, in macrophages proximate to adaptive immune cells secreting IFNγ, the activation of both GAF and IRF1 will reprogram the epigenome and trigger the formation of *de novo* enhancers.

Therefore, the mechanism by which IRF1 reprograms the epigenome is restricted to TLR-signaling and Type II IFN signaling, but not low doses of IFNβ, which only activates ISGF3. Low levels of tonic IFNβ maintain homeostasis in multiple tissues and confer a basal degree of antiviral protection (Gough et al. 2010; Kishimoto et al. 2021). We illustrate that only in an active infection, that is, in environments with high levels of IFNγ or IFNβ (which activates GAF), or in the infected cells themselves, will the macrophages generate *de novo* enhancers.

The chromatin state and epigenetic reprogramming dynamics observed for NFκB- or IRF- associated enhancers share remarkable similarities. This dissertation further extends existing literature on *de novo* enhancers in several significant ways. First, *de novo* enhancers acquire H3K4me1 marks that persist for up to 6-days after the removal of the stimuli, in contrast to other epigenetic marks such as H3K27ac, which decline after 24-hours. Second, half of these *de novo* enhancers are pre-occupied with PU.1 and exhibit increase recruitment upon stimulation. In the case of IRF-regulated enhancers, IRF1 is required at sites with lower PU.1 binding. Third, these *de novo* enhancers are not pre-primed with RNA polymerase II, distinguishing them from promoter regions that already have it pre-bound in naïve macrophages. These results suggest that *de novo* enhancer formation must undergo extensive chromatin remodeling by SDTFs NFκB and IRFs.

These studies also shed light on the roles of IRF3 and ISGF3 in the formation of enhancers. Previous investigations within our lab elucidated that in viral infections, IRF3 is required but not sufficient to initiate gene expression responses, while ISGF3 drives the innate defenses in the infected cell (Ourthiague et al. 2015). The studies presented in this dissertation further extends on that observation, revealing that only a subset of locations exhibit stronger IRF3 binding and a more pronounced deficiency in the *Irf3*$^{-/-}$ opening chromatin and gaining H3K4me1 marks. We find that the role of IRF3 in the formation of LPS-induced enhancers is indirect – as IRF3 is required for ISGF3 activation. We recognize that IRF7 might be compensating for the loss of IRF3 in *Irf3*$^{-/-}$ BMDMs. However, given the requirement for IRF1, we expect that the combined action of IRF3/7 is able to trigger enhancer formation only at a minority of locations. Knocking out IRF3 and IRF7 to elucidate the compensating mechanisms of IRF7 should be addressed in future work.

We demonstrate that ISGF3 alone is not sufficient to form enhancers. Our studies reveal that IRF1 is required to initiate chromatin opening, while ISGF3 requirement is apparent at later

stages. The enhancer locations that exhibited a stronger deficiency in the IRF1 knockout were also more closed in conformation, as shown by lower levels of chromatin accessibility and PU.1 and RNA polymerase II occupancy in naïve macrophages. ISGF3 is a trimeric complex comprised of IRF9, phosphorylated STAT1 and phosphorylated STAT2, forming a large complex of 250 kDa (Qureshi et al. 1995). We hypothesize that IRF1, being a much smaller protein (37kDa, potentially functioning as a monomer), is able to access these regions to initiate chromatin remodeling. ISGF3, being a larger complex, preferentially acts either in regions that are more open in conformation or that have been pre-opened by IRF1. Further *in vitro* studies are needed to contrast IRF1 and ISGF3 binding to close chromatin and ejecting nucleosomes.

In the context of IFNγ signaling, where ISGF3 inducibility was not detected, we demonstrated the cooperative action of IRF1 with GAF in forming *de novo* enhancers. The basal state of the IRF1-dependent enhancer regions showed less chromatin accessibility, histone modifications, and PU.1 binding compared to those that are IRF1-independent, suggesting a central role of IRF1 to initiate chromatin opening. Within the IFNγ-specific enhancers, we observed GAF and IRF1 binding to non-consensus sequences, indicating the potential for direct interaction between IRF1 and GAF at these regions. Indeed, previous studies have shown the formation of a complex between STAT1-IRF1 (Chatterjee-Kishore et al. 2000) or direct contact of STAT1 and IRF1 through chromatin looping (Abou El Hassan et al. 2017; Ni et al. 2008). Interestingly, we observed higher H3K27ac levels in enhancer regions that were bound by GAF. Other studies have previously reported that in the IFNγ response, STAT1 binds to sites that are preoccupied with IRF1, inducing remodeling of H3K27ac (Qiao et al. 2013). These results suggest that while IRF1 is needed to initiate chromatin opening, GAF is required to recruit enzymes that deposit enhancer marks.

We find a common set of enhancers induced by both LPS and IFNγ, which demonstrates a scenario where IRF1 can cooperate with either ISGF3 or GAF to generate

these enhancers. We show that there is a stronger deficiency by the loss of IRF1 in macrophages stimulated with IFNγ than with LPS, further supporting that IRF1 might be directly binding to GAF, as opposed to the sequential binding of IRF1-ISGF3.

The combinatorial versatility of IRF1 could also be based on the fact that both ISRE and GAS elements are composed of GAAA half-sites, arranged in the former as direct repeats and in the latter as palindromes. Thus, the arrangement of the two half-sites determines specificity for the partner transcription factor and just three such half-sites may allow either IFNβ-induced ISGF3 or IFNγ-induced GAF to synergize with IRF1 to open chromatin. There is additional flexibility here, as dimeric transcription factors often find sufficient binding energy at sites that contain a degenerate second half-site (Ngo et al 2020). This explains why not all ChIP-detected binding events even at high stringency identify full ISRE or GAS elements, but also suggests how IRF1 may cooperate with either interferon-induced SDTF and via either ISRE or GAS elements.

Generally, these *de novo* enhancers are thought to impact the response of macrophages to subsequent stimuli, and thus play a role in innate immune memory of macrophages (Ostuni et al. 2013; Saeed et al. 2014; Novakovic et al. 2016; Netea et al. 2020). However, how *de novo* enhancers actually do this, and to what extent, remains poorly understood. What is clear from the studies of enhancers in general is that enhancers often affect multiple genes, and that genes are usually regulated by many, often distantly located, enhancers. Thus, while direct mapping of an enhancer-promoter interaction has been reported in some cases (Ni et al. 2008), this does not convey the full picture of how enhancers regulate gene expression or the inducibility of gene expression when cells are stimulated again.

In both our previous manuscript focusing on NFκB-induced enhancers (Cheng et al. 2021), and this manuscript on IRF-induced enhancers, we show that there are genes whose inducibility is potentiated in a manner that correlates with enhancer formation, thus providing

some evidence that the IRF1-dependent *de novo* enhancers are functionally important for the innate immune training of macrophages. However, based on the current understanding in the enhancer field (and our own prior experience), it is likely that disrupting one enhancer (even good candidates that show proximity in 1D or 3D with promoters), has barely discernible effects on the expression of a specific gene, because its disruption may be compensated by many other enhancers or the effects are broad, affecting many genes, undermining confidence in its specificity. Further work to establish enhancer-gene interactions by mapping the 3D chromatin structure is required to analyze how *de novo* enhancers control gene expression responses.

The stimulus-induced expression of IRF1, mediated either by PAMP-induced NFκB or IFNγ-induced GAF, creates a combinatorial requirement for IRF1 and a partner SDTF. This ensures that *de novo* enhancers are selectively formed only in macrophages exposed directly to pathogens, which activate NFκB, or in proximity to adaptive immune cells secreting IFNγ. Consequently, macrophages exposed to paracrine type I interferon, despite inducing anti-viral and innate immune genes, do not undergo substantial epigenomic reprogramming.

The reprogramming of macrophages in disease scenarios has been explored for two distinct purposes; either to potentiate or to dampen innate immune responses. In clinical settings, sepsis patients treated with adjuvant immunotherapy using IFNγ exhibited clinical improvements (Payen et al. 2019). In addition, clinical trials exploring the use of TLR agonists in combination with immunotherapy have shown promise (Adams 2009). For instance, dendritic cell vaccination with TLR agonists enhanced type I and II IFN responses, leading to improved survival in glioblastoma patients (Everson et al. 2023).

Conversely, the hyperactivation of tissue resident macrophages in the brain is associated with diseases like multiple sclerosis or Alzheimer's disease (Rodriguez et al. 2019). Studies have demonstrated that microglia exposed to multiple doses of LPS enter a tolerant state, exhibiting increased resistance to neuronal damage compared to those receiving one

dose of LPS (Wendeln et al. 2018), and this was associated with differences in H3K4me1 and H3K27ac between the two immune memory states. These results suggest that the tolerant state prevents further exacerbation of stroke pathology, suggesting that in cases of neuroinflammatory diseases, targeting the epigenetic reprogramming of microglia could be exploited to slow disease progression.

Epigenetic reprogramming of innate immune cells is pivotal for developing innate immune memory associated with infections and chronic inflammation. While broad-spectrum epigenetic inhibitors exist, they often have systemic off-target effects. Therefore, exploring more targeted therapies, such as specifically targeting IRF1 in macrophages, holds promise for achieving more specific clinical outcomes in the context of innate immune memory and associated diseases.

CHAPTER 4: METHODS

CHAPTER 4: METHODS

4.1 Animals, cell culture, and stimuli

Wild-type and gene-deficient C57BL/6 mice were housed and handled according to guidelines established by the UCLA Animal Research Committee under protocols ARC-2014-110 and ARC-2014-126. Bone marrow was isolated and cells were grown as previously described (Luecke et al. 2023). Cells were stimulated on day 7 with 100ng/mL LPS (L6529-1MG, Sigma-Aldrich) or Lipid A, 1 U/mL IFNβ (12401-1, pbl assay science), or 100ng/mL IFNγ (485-MI R&D Systems) for the indicated times.

4.2 Biochemical analysis

Nuclear extracts were collected by previously described protocols (Luecke et al. 2023). For immuno-blots, the following antibodies were used: rabbit anti-IRF1 (Santa Cruz sc640), mouse anti-pSTAT1 (Santa Cruz sc136229), rabbit anti-pSTAT2 (Sigma-Aldrich 07-224), mouse anti-IRF9 (Millipore-Sigma MABS1920), or rabbit anti-p84 (Abcam ab131268), followed by mouse anti-rabbit IgG-HRP (Cell Signaling 7074) or anti-mouse IgG-HRP (Cell Signaling 7076). EMSA was performed as previously described (Luecke et al. 2023; Wilder et al. 2023). For the ISRE consensus sequence we used 5’-GATCCTCGGGAAAGGGAAACCTAAACTGAAGCC-3’ and 5’- GGCTTCAGTTTAGGTTTCCCTTTCCCGAGGATC-3’; for the GAS consensus sequence we used 5’-TACAACAGCCTGATTTCCCCGAAATGACGC-3’ and 5’-GCGTCATTTCGGGGAAATCAGGCTGTTGTA-3’; and for the NFY consensus sequence we used 5’-GATTTTTTCCTGATTGGTTAAA-3’ and 5’- ACTTTTAACCAATCAGGAAAAA-3’ as a loading control.

4.3 ChIP-seq analysis

Chromatin Immuno-precipitation was carried out using a previously described protocol (Cheng et al. 2021). ChIP-seq libraries were prepared using the NEBNext Ultra II DNA Library Prep Kit (New England Biolabs E7645). Libraries were single-end sequenced with a length of 50bp on an Illumina HiSeq 3000. Reads were processed and aligned to the mouse genome (mm10) as previously described (Cheng et al. 2021). MACS (MACS2/MACS3) (Zhang et al. 2008) was used to call peaks at 1% FDR.

We generated two reference peak files by merging the peaks in the LPS or IFNγ (+unstimulated control) conditions in WT cells. We used these genomic locations to count the fragments in the WT and knockout samples for each stimulus condition using deeptools multiBamSummary (Ramírez et al. 2016). edgeR (Robinson et al. 2010) was used to determine the significantly induced regions by applying a cutoff FDR < 0.05 and log2FC > 0.5 (LPS) or FDR <0.01 and log2FC > 0.5 (IFNγ) compared to the unstimulated condition in WT cells. For the IRF1 or IFNAR dependent groups in Figure 2, significant peaks were identified by applying a cutoff FDR <0.05 and log2FC > 0.5 in WT vs *Irf1*$^{-/-}$ or *Ifnar*$^{-/-}$ conditions, and the control group was identified by FDR > 0.8 in WT vs *Irf1*$^{-/-}$ and *Ifnar*$^{-/-}$ in the LPS inducible peaks. IRF1-dependent or -independent groups in Figure 4 were defined by applying a cutoff FDR < 0.05 and log2FC > 0.5 comparing duplicates of WT and *Irf1*$^{-/-}$ IFNγ-stimulated samples.

Analysis of *de novo* transcription factor motif enrichment was performed using findMotifsGenome function in the HOMER suite (Heinz et al. 2010), using all detected peaks in WT as background. Data were visualized with ggplot2 or the pheatmap packages in R.

The following ChIP-seq datasets on BMDMs were obtained from Gene Expression Omnibus: H3K27ac (LPS or IFNγ stimulation; GSE38377), PU.1 (LPS or IFNγ stimulation; GSE38377), RNA Polymerase II (LPS stimulation; GSE38377), IRF3 (Lipid A stimulation; GSE99895), IRF9 (IFNβ stimulation; GSE77886), IRF1 (LPS stimulation; GSE56123), IRF1 (IFNγ stimulation; GSE77886), STAT1 (IFNγ stimulation; GSE115435 and GSE33913) (Ostuni

et al. 2013; Tong et al. 2016; Platanitis et al. 2019; Mancino et al. 2015; Langlais et al. 2016; Ng et al. 2011). Raw datasets were aligned against mm10 as previously described (Cheng et al. 2021). MACS (MACS3) (Zhang et al. 2008) was used to call peaks at 1% FDR. A merged file was obtained for each transcription factor and overlaps with the stimulus-specific H3K4me1 peaks were determined using the intersect function of the Bedtools package (Quinlan and Hall 2010).

ATAC-seq analysis

ATAC was carried out using a previously described protocol (Cheng et al. 2021). Libraries were prepared using the Nextera DNA Library Preparation Kit (Illumina, FC-121) and single-end sequenced (50bp) on an Illumina HiSeq 3000. Sequenced reads were processed and aligned to the mouse genome (mm10) as previously described (Cheng et al. 2021). MACS (MACS2) (Zhang et al. 2008) was used to call peaks at 1% FDR. The peaks for all the ATAC-seq samples were used to generate a single reference peak file, and the number of reads that fell into each peak was counted using deeptools multiBamSummary (Ramírez et al. 2016). The overlap between the ATAC-seq and ChIP-seq peaks was determined using the intersect function of the Bedtools package (Quinlan and Hall 2010). Reads were normalized by RPKM. Data were visualized with ggplot2 or the pheatmap packages in R.

RNA-seq analysis

BMDMs were lysed with TRIzol reagent (Life Technologies), and total RNA was purified using DIRECTzol RNA miniprep kit (Zymo Research). RNA samples were submitted to BGI Genomics for selection of polyadenylated RNA and paired-end library preparation. Samples were sequenced on DNBSEQ Technology platform (100bp). Raw data was filtered for adapter sequences or low-quality sequences using SOAPnuke. Reads were aligned to the mm10 genome using STAR (Dobin et al. 2013). Aligned reads were processed as previously described

(Cheng et al. 2021). Data was normalized by TPM. Genes with a TPM > 5 in at least two conditions were selected. The LPS-inducible genes were determined by applying a cutoff LFC > 0.5 in at least one timepoint in the PBS, IFNγ, or LPS conditions. The closest genes to the IFNγ enhancers and the LPS-inducible genes within +/- 100 kilobase were based on linear proximity to the transcription start sites (TSSs). Data were visualized with ggplot2 or the pheatmap packages in R.

BIBLIOGRAPHY

Abou El Hassan M, Huang K, Eswara MBK, Xu Z, Yu T, Aubry A, Ni Z, Livne-bar I, Sangwan M, Ahmad M, et al. 2017. Properties of STAT1 and IRF1 enhancers and the influence of SNPs. *BMC Molecular Biol* **18**: 6.

Adams S. 2009. Toll-like receptor agonists in cancer therapy. *Immunotherapy* **1**: 949–964.

Ahmed NS, Gatchalian J, Ho J, Burns MJ, Hah N, Wei Z, Downes M, Evans RM, Hargreaves DC. 2022. BRD9 regulates interferon-stimulated genes during macrophage activation via cooperation with BET protein BRD4. *Proc Natl Acad Sci U S A* **119**: e2110812119.

Alfarano G, Audano M, Di Chiaro P, Balestrieri C, Milan M, Polletti S, Spaggiari P, Zerbi A, Diaferia GR, Mitro N, et al. 2023. Interferon regulatory factor 1 (IRF1) controls the metabolic programmes of low-grade pancreatic cancer cells. *Gut* **72**: 109–128.

Bistoni F, Vecchiarelli A, Cenci E, Puccetti P, Marconi P, Cassone A. 1986. Evidence for macrophage-mediated protection against lethal Candida albicans infection. *Infect Immun* **51**: 668–674.

Biswas SK, Lopez-Collazo E. 2009. Endotoxin tolerance: new mechanisms, molecules and clinical significance. *Trends in Immunology* **30**: 475–487.

Charles A Janeway J, Travers P, Walport M, Shlomchik MJ. 2001. The importance of immunological memory in fixing adaptive immunity in the genome. In *Immunobiology: The Immune System in Health and Disease. 5th edition*, Garland Science https://www.ncbi.nlm.nih.gov/books/NBK27087/ (Accessed December 6, 2023).

Chatterjee-Kishore M, Wright KL, Ting JP-Y, Stark GR. 2000. How Stat1 mediates constitutive gene expression: a complex of unphosphorylated Stat1 and IRF1 supports transcription of the LMP2 gene. *The EMBO Journal* **19**: 4111–4122.

Chen S, Yang J, Wei Y, Wei X. 2020. Epigenetic regulation of macrophages: from homeostasis maintenance to host defense. *Cell Mol Immunol* **17**: 36–49.

Cheng Q, Behzadi F, Sen S, Ohta S, Spreafico R, Teles R, Modlin RL, Hoffmann A. 2019. Sequential conditioning-stimulation reveals distinct gene- and stimulus-specific effects of Type I and II IFN on human macrophage functions. *Sci Rep* **9**: 5288.

Cheng QJ, Ohta S, Sheu KM, Spreafico R, Adelaja A, Taylor B, Hoffmann A. 2021. NF-κB dynamics determine the stimulus specificity of epigenomic reprogramming in macrophages. *Science* **372**: 1349–1353.

Cohen B, Peretz D, Vaiman D, Benech P, Chebath J. 1988. Enhancer-like interferon responsive sequences of the human and murine (2′-5′) oligoadenylate synthetase gene promoters. *The EMBO Journal* **7**: 1411–1419.

Comoglio F, Simonatto M, Polletti S, Liu X, Smale ST, Barozzi I, Natoli G. 2019. Dissection of acute stimulus-inducible nucleosome remodeling in mammalian cells. *Genes Dev* **33**: 1159–1174.

Csumita M, Csermely A, Horvath A, Nagy G, Monori F, Göczi L, Orbea H-A, Reith W, Széles L. 2020. Specific enhancer selection by IRF3, IRF5 and IRF9 is determined by ISRE half-sites, 5′ and 3′ flanking bases, collaborating transcription factors and the chromatin environment in a combinatorial fashion. *Nucleic Acids Research* **48**: 589–604.

Decker T, Kovarik P, Meinke A. 1997. GAS Elements: A Few Nucleotides with a Major Impact on Cytokine-Induced Gene Expression. *Journal of Interferon & Cytokine Research* **17**: 121–134.

Dobin A, Davis CA, Schlesinger F, Drenkow J, Zaleski C, Jha S, Batut P, Chaisson M, Gingeras TR. 2013. STAR: ultrafast universal RNA-seq aligner. *Bioinformatics* **29**: 15–21.

Everson RG, Hugo W, Sun L, Antonios J, Lee A, Ding L, Bu M, Khattab S, Chavez C, Billingslea-Yoon E, et al. 2023. Dendritic Cell Vaccination in Conjunction with a TLR Agonist Polarizes Interferon Immune Responses in Malignant Glioma Patients. *Res Sq* rs.3.rs-3287211.

Foster SL, Hargreaves DC, Medzhitov R. 2007. Gene-specific control of inflammation by TLR-induced chromatin modifications. *Nature* **447**: 972–978.

Fujii Y. 1999. Crystal structure of an IRF-DNA complex reveals novel DNA recognition and cooperative binding to a tandem repeat of core sequences. *The EMBO Journal* **18**: 5028–5041.

Fujita T, Sakakibara J, Miyamoto M, Kimura Y, Taniguchi T. 1988. Evidence for a nuclear factor(s), IRF-1, mediating induction and silencing properties to human IFN-,B gene regulatory elements.

Ghisletti S, Barozzi I, Mietton F, Polletti S, De Santa F, Venturini E, Gregory L, Lonie L, Chew A, Wei C-L, et al. 2010. Identification and Characterization of Enhancers Controlling the Inflammatory Gene Expression Program in Macrophages. *Immunity* **32**: 317–328.

Gough DJ, Messina NL, Hii L, Gould JA, Sabapathy K, Robertson APS, Trapani JA, Levy DE, Hertzog PJ, Clarke CJP, et al. 2010. Functional Crosstalk between Type I and II Interferon through the Regulated Expression of STAT1 ed. S.W. Virgin. *PLoS Biol* **8**: e1000361.

Heinz S, Benner C, Spann N, Bertolino E, Lin YC, Laslo P, Cheng JX, Murre C, Singh H, Glass CK. 2010. Simple Combinations of Lineage-Determining Transcription Factors Prime cis-Regulatory Elements Required for Macrophage and B Cell Identities. *Molecular Cell* **38**: 576–589.

Honda K, Takaoka A, Taniguchi T. 2006. Type I Inteferon Gene Induction by the Interferon Regulatory Factor Family of Transcription Factors. *Immunity* **25**: 349–360.

Ivashkiv LB. 2018. IFNγ: signalling, epigenetics and roles in immunity, metabolism, disease and cancer immunotherapy. *Nat Rev Immunol* **18**: 545–558.

Ivashkiv LB, Donlin LT. 2014. Regulation of type I interferon responses. *Nat Rev Immunol* **14**: 36–49.

Kaikkonen MU, Spann NJ, Heinz S, Romanoski CE, Allison KA, Stender JD, Chun HB, Tough DF, Prinjha RK, Benner C, et al. 2013. Remodeling of the Enhancer Landscape during Macrophage Activation Is Coupled to Enhancer Transcription. *Molecular Cell* **51**: 310–325.

Kang K, Bachu M, Park SH, Kang K, Bae S, Park-Min K-H, Ivashkiv LB. 2019. IFN-γ selectively suppresses a subset of TLR4-activated genes and enhancers to potentiate macrophage activation. *Nat Commun* **10**: 3320.

Kaufmann E, Khan N, Tran KA, Ulndreaj A, Pernet E, Fontes G, Lupien A, Desmeules P, McIntosh F, Abow A, et al. 2022. BCG vaccination provides protection against IAV but not SARS-CoV-2. *Cell Reports* **38**: 110502.

Kawai T, Akira S. 2010. The role of pattern-recognition receptors in innate immunity: update on Toll-like receptors. *Nat Immunol* **11**: 373–384.

Kim J, Sheu KM, Cheng QJ, Hoffmann A, Enciso G. 2022. Stochastic models of nucleosome dynamics reveal regulatory rules of stimulus-induced epigenome remodeling. *Cell Reports* **40**: 111076.

Kim J, Venkata NC, Hernandez Gonzalez GA, Khanna N, Belmont AS. 2019. Gene expression amplification by nuclear speckle association. *J Cell Biol* **219**: e201904046.

Kishimoto K, Wilder CL, Buchanan J, Nguyen M, Okeke C, Hoffmann A, Cheng QJ. 2021. High Dose IFN-β Activates GAF to Enhance Expression of ISGF3 Target Genes in MLE12 Epithelial Cells. *Front Immunol* **12**: 651254.

Langlais D, Barreiro LB, Gros P. 2016. The macrophage IRF8/IRF1 regulome is required for protection against infections and is associated with chronic inflammation. *Journal of Experimental Medicine* **213**: 585–603.

Luecke S, Adelaja A, Guo X, Sen S, Spreafico R, Singh A, Liu Y, Taylor B, Diaz J, Cheng Q, et al. 2023. Tonic TNF conditioning of macrophages safeguards stimulus-specific inflammatory responses. *EMBO Reports* **24**: e55986.

Mancino A, Termanini A, Barozzi I, Ghisletti S, Ostuni R, Prosperini E, Ozato K, Natoli G. 2015. A dual *cis* -regulatory code links IRF8 to constitutive and inducible gene expression in macrophages. *Genes Dev* **29**: 394–408.

Mayran A, Drouin J. 2018. Pioneer transcription factors shape the epigenetic landscape. *Journal of Biological Chemistry* **293**: 13795–13804.

Michalska A, Blaszczyk K, Wesoly J, Bluyssen HAR. 2018. A Positive Feedback Amplifier Circuit That Regulates Interferon (IFN)-Stimulated Gene Expression and Controls Type I and Type II IFN Responses. *Front Immunol* **9**: 1135.

Miyamoto M, Fujita T, Kimura Y, Maruyama M, Harada H, Sudo Y, Miyata T, Taniguchi T. 1988. Regulated expression of a gene encoding a nuclear factor, IRF-1, that specifically binds to IFN-beta gene regulatory elements. *Cell* **54**: 903–913.

Murray PJ, Wynn TA. 2011. Protective and pathogenic functions of macrophage subsets. *Nat Rev Immunol* **11**: 723–737.

Näf D, Hardin SE, Weissmann C. 1991. Multimerization of AAGTGA and GAAAGT generates sequences that mediate virus inducibility by mimicking an interferon promoter element. *Proc Natl Acad Sci USA* **88**: 1369–1373.

Netea MG, Domínguez-Andrés J, Barreiro LB, Chavakis T, Divangahi M, Fuchs E, Joosten LAB, van der Meer JWM, Mhlanga MM, Mulder WJM, et al. 2020. Defining trained immunity and its role in health and disease. *Nat Rev Immunol* **20**: 375–388.

Netea MG, Joosten LAB, Latz E, Mills KHG, Natoli G, Stunnenberg HG, O'Neill LAJ, Xavier RJ. 2016. Trained immunity: A program of innate immune memory in health and disease. *Science* **352**: aaf1098.

Ng S-L, Friedman BA, Schmid S, Gertz J, Myers RM, tenOever BR, Maniatis T. 2011. IκB kinase ε (IKKε) regulates the balance between type I and type II interferon responses. *Proc Natl Acad Sci USA* **108**: 21170–21175.

Ni Z, Hassan MAE, Xu Z, Yu T, Bremner R. 2008. The chromatin-remodeling enzyme BRG1 coordinates CIITA induction through many interdependent distal enhancers. *Nat Immunol* **9**: 785–793.

Novakovic B, Habibi E, Wang S-Y, Arts RJW, Davar R, Megchelenbrink W, Kim B, Kuznetsova T, Kox M, Zwaag J, et al. 2016. β-Glucan Reverses the Epigenetic State of LPS-Induced Immunological Tolerance. *Cell* **167**: 1354-1368.e14.

Ostuni R, Piccolo V, Barozzi I, Polletti S, Termanini A, Bonifacio S, Curina A, Prosperini E, Ghisletti S, Natoli G. 2013. Latent enhancers activated by stimulation in differentiated cells. *Cell* **152**: 157–171.

Ourthiague DR, Birnbaum H, Ortenlöf N, Vargas JD, Wollman R, Hoffmann A. 2015. Limited specificity of IRF3 and ISGF3 in the transcriptional innate-immune response to double-stranded RNA. *J Leukoc Biol* **98**: 119–128.

Payen D, Faivre V, Miatello J, Leentjens J, Brumpt C, Tissières P, Dupuis C, Pickkers P, Lukaszewicz AC. 2019. Multicentric experience with interferon gamma therapy in sepsis induced immunosuppression. A case series. *BMC Infect Dis* **19**: 931.

Pine R. 1997. Convergence of TNFα and IFNγ signalling pathways through synergistic induction of IRF-1/ISGF-2 is mediated by a composite GAS/κB promoter element.

Platanitis E, Demiroz D, Schneller A, Fischer K, Capelle C, Hartl M, Gossenreiter T, Müller M, Novatchkova M, Decker T. 2019. A molecular switch from STAT2-IRF9 to ISGF3 underlies interferon-induced gene transcription. *Nat Commun* **10**: 2921.

Platanitis E, Gruener S, Ravi Sundar Jose Geetha A, Boccuni L, Vogt A, Novatchkova M, Sommer A, Barozzi I, Müller M, Decker T. 2022b. Interferons reshape the 3D conformation and accessibility of macrophage chromatin. *iScience* **25**: 103840.

Qiao Y, Giannopoulou EG, Chan CH, Park S, Gong S, Chen J, Hu X, Elemento O, Ivashkiv LB. 2013. Synergistic Activation of Inflammatory Cytokine Genes by Interferon-γ-Induced Chromatin Remodeling and Toll-like Receptor Signaling. *Immunity* **39**: 454–469.

Quinlan AR, Hall IM. 2010. BEDTools: a flexible suite of utilities for comparing genomic features. *Bioinformatics* **26**: 841–842.

Quintin J, Saeed S, Martens JHA, Giamarellos-Bourboulis EJ, Ifrim DC, Logie C, Jacobs L, Jansen T, Kullberg B-J, Wijmenga C, et al. 2012. Candida albicans Infection Affords Protection against Reinfection via Functional Reprogramming of Monocytes. *Cell Host & Microbe* **12**: 223–232.

Qureshi SA, Salditt-Georgieff M, Darnell JE. 1995. Tyrosine-phosphorylated Stat1 and Stat2 plus a 48-kDa protein all contact DNA in forming interferon-stimulated-gene factor 3. *Proc Natl Acad Sci U S A* **92**: 3829–3833.

Ramírez F, Ryan DP, Grüning B, Bhardwaj V, Kilpert F, Richter AS, Heyne S, Dündar F, Manke T. 2016. deepTools2: a next generation web server for deep-sequencing data analysis. *Nucleic Acids Res* **44**: W160-165.

Ramsauer K, Farlik M, Zupkovitz G, Seiser C, Kröger A, Hauser H, Decker T. 2007. Distinct modes of action applied by transcription factors STAT1 and IRF1 to initiate transcription of the IFN-γ-inducible *gbp2* gene. *Proc Natl Acad Sci USA* **104**: 2849–2854.

Robinson MD, McCarthy DJ, Smyth GK. 2010. edgeR: a Bioconductor package for differential expression analysis of digital gene expression data. *Bioinformatics* **26**: 139–140.

Rodriguez RM, Suarez-Alvarez B, Lopez-Larrea C. 2019. Therapeutic Epigenetic Reprogramming of Trained Immunity in Myeloid Cells. *Trends in Immunology* **40**: 66–80.

Rosain J, Neehus A-L, Manry J, Yang R, Le Pen J, Daher W, Liu Z, Chan Y-H, Tahuil N, Türel Ö, et al. 2023. Human IRF1 governs macrophagic IFN-γ immunity to mycobacteria. *Cell* **186**: 621-645.e33.

Saeed S, Quintin J, Kerstens HHD, Rao NA, Aghajanirefah A, Matarese F, Cheng S-C, Ratter J, Berentsen K, van der Ent MA, et al. 2014. Epigenetic programming of monocyte-to-macrophage differentiation and trained innate immunity. *Science* **345**: 1251086.

Sakaguchi S, Negishi H, Asagiri M, Nakajima C, Mizutani T, Takaoka A, Honda K, Taniguchi T. 2003. Essential role of IRF-3 in lipopolysaccharide-induced interferon-β gene expression and endotoxin shock. *Biochemical and Biophysical Research Communications* **306**: 860–866.

Sato M, Hata N, Asagiri M, Nakaya T, Taniguchi T, Tanaka N. 1998. Positive feedback regulation of type I IFN genes by the IFN-inducible transcription factor IRF-7. *FEBS Lett* **441**: 106–110.

Schmid S, Mordstein M, Kochs G, García-Sastre A, tenOever BR. 2010. Transcription Factor Redundancy Ensures Induction of the Antiviral State. *Journal of Biological Chemistry* **285**: 42013–42022.

Sekrecka A, Kluzek K, Sekrecki M, Boroujeni ME, Hassani S, Yamauchi S, Sada K, Wesoly J, Bluyssen HAR. 2023. Time-dependent recruitment of GAF, ISGF3 and IRF1 complexes shapes IFNα and IFNγ-activated transcriptional responses and explains mechanistic and functional overlap. *Cell Mol Life Sci* **80**: 187.

Sheu K, Luecke S, Hoffmann A. 2019. Stimulus-specificity in the Responses of Immune Sentinel Cells. *Curr Opin Syst Biol* **18**: 53–61.

Shi L, Perin JC, Leipzig J, Zhang Z, Sullivan KE. 2011. Genome-wide analysis of interferon regulatory factor I binding in primary human monocytes. *Gene* **487**: 21–28.

Shin J, Toyoda S, Nishitani S, Onodera T, Fukuda S, Kita S, Fukuhara A, Shimomura I. 2022. SARS-CoV-2 infection impairs the insulin/IGF signaling pathway in the lung, liver, adipose tissue, and pancreatic cells via IRF1. *Metabolism* **133**: 155236.

Song R, Gao Y, Dozmorov I, Malladi V, Saha I, McDaniel MM, Parameswaran S, Liang C, Arana C, Zhang B, et al. 2021. IRF1 governs the differential interferon-stimulated gene responses in human monocytes and macrophages by regulating chromatin accessibility. *Cell Rep* **34**: 108891.

Tamura T, Yanai H, Savitsky D, Taniguchi T. 2008. The IRF Family Transcription Factors in Immunity and Oncogenesis. *Annu Rev Immunol* **26**: 535–584.

Taniguchi T, Ogasawara K, Takaoka A, Tanaka N. 2001. IRF Family of Transcription Factors as Regulators of Host Defense. *Annu Rev Immunol* **19**: 623–655.

Tong A-J, Liu X, Thomas BJ, Lissner MM, Baker MR, Senagolage MD, Allred AL, Barish GD, Smale ST. 2016. A Stringent Systems Approach Uncovers Gene-Specific Mechanisms Regulating Inflammation. *Cell* **165**: 165–179.

van der Heijden CDCC, Noz MP, Joosten LAB, Netea MG, Riksen NP, Keating ST. 2018. Epigenetics and Trained Immunity. *Antioxidants & Redox Signaling* **29**: 1023–1040.

Wendeln A-C, Degenhardt K, Kaurani L, Gertig M, Ulas T, Jain G, Wagner J, Häsler LM, Wild K, Skodras A, et al. 2018. Innate immune memory in the brain shapes neurological disease hallmarks. *Nature* **556**: 332–338.

Wilder CL, Lefaudeux D, Mathenge R, Kishimoto K, Zuniga Munoz A, Nguyen MA, Meyer AS, Cheng QJ, Hoffmann A. 2023. A stimulus-contingent positive feedback loop enables IFN-β dose-dependent activation of pro-inflammatory genes. *Molecular Systems Biology* **19**: e11294.

Yanai H, Negishi H, Taniguchi T. 2012. The IRF family of transcription factors: Inception, impact and implications in oncogenesis. *Oncoimmunology* **1**: 1376–1386.

Yildirim A, Boninsegna L, Zhan Y, Alber F. 2022. Uncovering the Principles of Genome Folding by 3D Chromatin Modeling. *Cold Spring Harb Perspect Biol* **14**: a039693.

Yoshida K, Maekawa T, Zhu Y, Renard-Guillet C, Chatton B, Inoue K, Uchiyama T, Ishibashi K, Yamada T, Ohno N, et al. 2015. The transcription factor ATF7 mediates lipopolysaccharide-induced epigenetic changes in macrophages involved in innate immunological memory. *Nat Immunol* **16**: 1034–1043.

Zhang Y, Liu T, Meyer CA, Eeckhoute J, Johnson DS, Bernstein BE, Nusbaum C, Myers RM, Brown M, Li W, et al. 2008. Model-based analysis of ChIP-Seq (MACS). *Genome Biol* **9**: R137.

Zhang Z, Shi L, Song L, Ephrem E, Petri M, Sullivan KE. 2015. Interferon Regulatory Factor 1 Marks Activated Genes and Can Induce Target Gene Expression in Systemic Lupus Erythematosus: IRF-1 in SLE. *Arthritis & Rheumatology* **67**: 785–796.

Zhao G-N, Jiang D-S, Li H. 2015. Interferon regulatory factors: at the crossroads of immunity, metabolism, and disease. *Biochim Biophys Acta* **1852**: 365–378.

Ziogas A, Netea MG. 2022. Trained immunity-related vaccines: innate immune memory and heterologous protection against infections. *Trends in Molecular Medicine* **28**: 497–512.